20. **Lenda DM, Kikawada E, Stanley ER, Kelley VR.** Reduced macrophage recruitment, proliferation, and activation in colony-stimulating factor-1-deficient mice results in decreased tubular apoptosis during renal inflammation. *J Immunol* 170: 3254–3262, 2003.
21. **Marumo T, Hishikawa K, Yoshikawa M, Fujita T.** Epigenetic regulation of BMP7 in the regenerative response to ischemia. *J Am Soc Nephrol* 19: 1311–1320, 2008.
22. **Marumo T, Uchimura H, Hayashi M, Hishikawa K, Fujita T.** Aldosterone impairs bone marrow-derived progenitor cell formation. *Hypertension* 48: 490–496, 2006.
23. **Mathew S, Tustison KS, Sugatani T, Chaudhary LR, Rifas L, Hruska KA.** The mechanism of phosphorus as a cardiovascular risk factor in CKD. *J Am Soc Nephrol* 19: 1092–1105, 2008.
24. **Mejat A, Ramond F, Bassel-Duby R, Khochbin S, Olson EN, Schaeffer L.** Histone deacetylase 9 couples neuronal activity to muscle chromatin acetylation and gene expression. *Nat Neurosci* 8: 313–321, 2005.
25. **Minetti GC, Colussi C, Adami R, Serra C, Mozzetta C, Parente V, Fortuni S, Straino S, Sampaolesi M, Di Padova M, Illi B, Gallinari P, Steinkuhler C, Capogrossi MC, Sartorelli V, Bottinelli R, Gaetano C, Puri PL.** Functional and morphological recovery of dystrophic muscles in mice treated with deacetylase inhibitors. *Nat Med* 12: 1147–1150, 2006.
26. **Mishra N, Reilly CM, Brown DR, Ruiz P, Gilkeson GS.** Histone deacetylase inhibitors modulate renal disease in the MRL-lpr/lpr mouse. *J Clin Invest* 111: 539–552, 2003.
27. **Montgomery RL, Potthoff MJ, Haberland M, Qi X, Matsuzaki S, Humphries KM, Richardson JA, Bassel-Duby R, Oslon EN.** Maintenance of cardiac energy metabolism by histone deacetylase 3 in mice. *J Clin Invest* 118: 3588–3597, 2008.
28. **Nott A, Watson PM, Robinson JD, Crepaldi L, Riccio A.** S-nitrosylation of histone deacetylase 2 induces chromatin remodelling in neurons. *Nature* 455: 411–415, 2008.
29. **Pandey UB, Nie Z, Batlevi Y, McCray BA, Ritson GP, Nedelsky NB, Schwartz SL, DiProspero NA, Knight MA, Schuldiner O, Padmanabhan R, Hild M, Berry DL, Garza D, Hubbert CC, Yao TP, Baehrecke EH, Taylor JP.** HDAC6 rescues neurodegeneration and provides an essential link between autophagy and the UPS. *Nature* 447: 859–863, 2007.
30. **Reddy P, Sun Y, Toubai T, Duran-Struuck R, Clouthier SG, Weisiger E, Maeda Y, Tawara I, Krijanovski O, Gatza E, Liu C, Malter C, Mascagni P, Dinarello CA, Ferrara JL.** Histone deacetylase inhibition modulates indoleamine 2,3-dioxygenase-dependent DC functions and regulates experimental graft-versus-host disease in mice. *J Clin Invest* 118: 2562–2573, 2008.
31. **Ricardo SD, van Goor H, Eddy AA.** Macrophage diversity in renal injury and repair. *J Clin Invest* 118: 3522–3530, 2008.
32. **Sakamoto S, Potla R, Larner AC.** Histone deacetylase activity is required to recruit RNA polymerase II to the promoters of selected interferon-stimulated early response genes. *J Biol Chem* 279: 40362–40367, 2004.
33. **Seligson DB, Horvath S, Shi T, Yu H, Tze S, Grunstein M, Kurdistani SK.** Global histone modification patterns predict risk of prostate cancer recurrence. *Nature* 435: 1262–1266, 2005.
34. **Tang H, Macpherson P, Marvin M, Meadows E, Klein WH, Yang XJ, Goldman D.** A histone deacetylase 4/myogenin positive feedback loop coordinates denervation-dependent gene induction and suppression. *Mol Biol Cell* 20: 1120–1131, 2009.
35. **Tao R, de Zoeten EF, Ozkaynak E, Chen C, Wang L, Porrett PM, Li B, Turka LA, Olson EN, Greene MI, Wells AD, Hancock WW.** Deacetylase inhibition promotes the generation and function of regulatory T cells. *Nat Med* 13: 1299–1307, 2007.
36. **Trivedi CM, Luo Y, Yin Z, Zhang M, Zhu W, Wang T, Floss T, Goettlicher M, Noppinger PR, Wurst W, Ferrari VA, Abrams CS, Gruber PJ, Epstein JA.** Hdac2 regulates the cardiac hypertrophic response by modulating Gsk3beta activity. *Nat Med* 13: 324–331, 2007.
37. **Uchimura H, Marumo T, Takase O, Kawachi H, Shimizu F, Hayashi M, Saruta T, Hishikawa K, Fujita T.** Intrarenal injection of bone marrow-derived angiogenic cells reduces endothelial injury and mesangial cell activation in experimental glomerulonephritis. *J Am Soc Nephrol* 16: 997–1004, 2005.
38. **Urbich C, Rossig L, Kaluza D, Potente M, Boeckel JN, Knau A, Diehl F, Geng JG, Hofmann WK, Zeiher AM, Dimmeler S.** HDAC5 is a repressor of angiogenesis and determines the angiogenic gene expression pattern of endothelial cells. *Blood* 113: 5669–5679, 2009.
39. **Xu WS, Parmigiani RB, Marks PA.** Histone deacetylase inhibitors: molecular mechanisms of action. *Oncogene* 26: 5541–5552, 2007.
40. **Yamaguchi K, Lantowski A, Dannenberg AJ, Subbaramaiah K.** Histone deacetylase inhibitors suppress the induction of c-Jun and its target genes including COX-2. *J Biol Chem* 280: 32569–32577, 2005.
41. **Yang J, Shultz RW, Mars WM, Wegner RE, Li Y, Dai C, Nejak K, Liu Y.** Disruption of tissue-type plasminogen activator gene in mice reduces renal interstitial fibrosis in obstructive nephropathy. *J Clin Invest* 110: 1525–1538, 2002.
42. **Yoshikawa M, Hishikawa K, Marumo T, Fujita T.** Inhibition of histone deacetylase activity suppresses epithelial-to-mesenchymal transition induced by TGF-beta1 in human renal epithelial cells. *J Am Soc Nephrol* 18: 58–65, 2007.

Jpn. J. Infect. Dis., 63, 67-71, 2010

Short Communication

The First Autopsy Case of Pandemic Influenza (A/H1N1pdm) Virus Infection in Japan: Detection of a High Copy Number of the Virus in Type II Alveolar Epithelial Cells by Pathological and Virological Examination

Noriko Nakajima[1], Satoru Hata[2], Yuko Sato[1], Minoru Tobiume[1], Harutaka Katano[1], Keiko Kaneko[1], Noriyo Nagata[1], Michiyo Kataoka[1], Akira Ainai[3], Hideki Hasegawa[1,3], Masato Tashiro[3], Makoto Kuroda[4], Tamami Odai[5], Nobuyuki Urasawa[5], Tomoyoshi Ogino[6], Hiroaki Hanaoka[6], Masahide Watanabe[6], and Tetsutaro Sata[1]*

[1]Department of Pathology, [3]Influenza Virus Research Center, and [4]Pathogen Genomics Center, National Institute of Infectious Diseases, Tokyo 162-8640; and [2]Department of Clinical Laboratory, [5]Department of Cardiology, and [6]Department of Pathology, Nagano Red Cross Hospital, Nagano 380-8582, Japan

(Received December 15, 2009. Accepted January 5, 2010)

SUMMARY: We report the pathological and virological findings of the first autopsy case of the 2009 pandemic influenza (A/H1N1pdm) virus infection in Japan. A man aged 33 years with chronic heart failure due to dilated cardiomyopathy, mild diabetes mellitus, atopic dermatitis, bronchial asthma, and obesity died of respiratory failure and multiple organ dysfunction syndrome. Macroscopic examination showed severe plumonary edema and microscopically the lung sections showed very early exudative-stage diffuse alveolar damage (DAD). Immunohistochemistry revealed proliferation of the influenza (A/H1N1pdm) virus in alveolar epithelial cells, some of which expressed SAα2-3Gal on the cell surface. Influenza (A/H1N1pdm) virus genomic RNA and mRNA were also detected in alveolar epithelial cells. Real-time PCR revealed 723 copies/cell in the left lower lung section from which the influenza (A/H1N1pdm) virus was isolated. Electron microscopic analysis revealed filamentous viral particles in the lung tissue. The concentrations of various cytokines/chemokines in the serum and the autopsied lung tissue were measured. IL-2R, IL-6, IL-8, IL-10, IFN-α, MCP-1, and MIG levels were elevated in both. These findings indicated a case of viral pneumonia caused by influenza (A/H1N1pdm) virus infection, showing characteristic pathological findings of the early stage of DAD.

The 2009 pandemic influenza (A/H1N1pdm) virus causes severe respiratory disease, neurologic complications, and myocardial symptom in some patients (1–3). From August 15 through December 15, 2009, a total of 116 patients with confirmed infection with influenza (A/H1N1pdm) virus died in Japan (4). Autopsy verification of the cause of death is indispensable to elucidate the pathogenesis of influenza (A/H1N1pdm) virus infection. Pathological findings of fatal influenza (A/H1N1pdm) virus infection have recently been reported (5,6). Here, we report in detail the pathological and virological findings of the first autopsy case in Japan.

On August 20, 2009 (day 1), a man aged 33 years with chronic heart failure due to dilated cardiomyopathy, mild diabetes mellitus, atopic dermatitis, asthma, and obesity (BMI, 38) complained of cough and watery diarrhea. On day 6, he was admitted with progressive dyspnea, high fever (39°C) and diarrhea. On admission, a chest radiogragh showed nodular infiltrates in the lower lungs (Fig. 1a) and a chest computed tomography (CT) scan revealed severe bilateral consolidations (Fig. 1b). The leukocyte count was 5,210/mm^3 and CRP was 1.1 mg/dl. The nasopharyngeal swab specimens were negative for influenza virus type A antigen by the rapid test (ESPLINE® Influenza A&B Kit; Fujirebio, Tokyo, Japan), and therefore oseltamivir was not administered. On the morning of day 7, the patient required intubation and was placed on mechanical ventilation. At intubation, foamy, white and partly bloody fluid spouted out from the tube. Methylprednisolone pulse therapy and administration of a neutrophil elastase inhibitor (sivelestat sodium hydrate) were initiated for the treatment of acute respiratory distress syndrome (ARDS). The diagnosis of influenza (A/H1N1pdm) virus infection was confirmed by real-time reverse transcriptase-polymerase chain reaction (RT-PCR) testing on day 7. In spite of intensive care, the patient died of respiratory failure and multiple organ dysfunction syndrome on day 8. The chest radiograph showed progressive and confluent consolidations (Fig. 1c).

Autopsy revealed macroscopically severe pulmonary edema, hemorrhage, exudation and focal nodular lesions in the lungs (left, 730 g; right, 800 g) (Fig. 2a). The bilateral main bronchi were filled with foamy liquid, which was positive for influenza virus A antigen. The nodular lesions were palpable in the lower lungs, and corresponded to the nodular shadows of the chest radiographic findings (Fig. 1c). The heart was enlarged and all chambers were dilated (670 g), and the left ventricular wall and septal wall had irregular whitish patches, compatible with dilated cardiomyopathy (Figs. 2b and c). The brain was edematous and swollen (1,350 g). Hyperplastic solitary lymph follicles of the terminal ileum and rectal erosion were observed.

Tissue samples from all major organs were fixed in 20% buffered formalin and embedded in paraffin by an automated

*Corresponding author: Mailing address: Department of Pathology, National Institute of Infectious Diseases, 1-23-1 Toyama, Shinjuku-ku, Tokyo 162-8640, Japan. Tel: +81-3-5285-1111, Fax: +81-3-5285-1189, E-mail: tsata@nih.go.jp

processor (SAKURA ETV-150CV; Sakura Finetek Japan, Tokyo, Japan). Each section was cut into 3 μm in thickness, mounted on silane-coated slides (Matsunami, Tokyo, Japan) and was examined histologically. Hematoxylin and eosin-stained lung sections demonstrated intra-alveolar edema with fibrin, erythrocytes and desquamated epithelial cells in alveolar spaces, hyperplasia of type II pneumocytes, and hemosiderin-laden macrophages (heart failure cells) (Figs. 3a, b, c, d, and e). No viral inclusion bodies or cytopathic changes were observed in pneumocytes. Neutrophil infiltration was not prominent. Regenerative hyperplasia and desquamation of the pseudostratified columnar epithelium of the bronchi were observed (Fig. 3a). Some sections demonstrated the feature of early exudative-stage diffuse alveolar damage (DAD) with hyaline membrane formation (Fig. 3c). The findings of more progressed proliferative-stage DAD were also observed in a few sections (Fig. 3e).

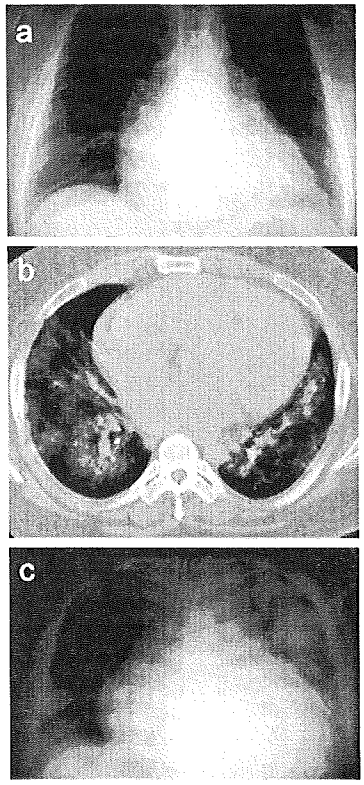

Fig. 1. Radiograph of the lung and chest computed tomography (CT). (a) The radiograph showed nodular infiltrates in lower lungs on day 6. (b) The chest CT scan revealed severe bilateral consolidations on day 6. (c) The radiograph showed progressive and confluent consolidations on day 8.

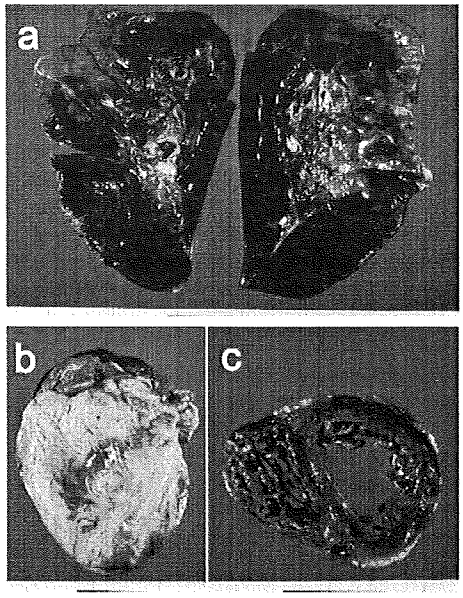

Fig. 2. Macroscopical findings. (a) Plumonary edema (left, 730 g; right, 800 g). (b, c) Enlarged heart (670 g) and dilated chambers compatible with dilated cardiomyopathy.

To evaluate the distribution of influenza (A/H1N1pdm) virus antigen, all sections were immunostained by an avidin-biotin complex immunoperoxidase method (LSAB2 kit/HRP/DAB; Dako Cytomation, Copenhagen, Denmark) using a mouse monoclonal antibody against influenza A nucleoprotein (InfA-NP) (7). Positive signals for InfA-NP antigen were detected primarily in the lung field sections, and only sparsely in a bronchial section (Figs. 3f, g, h, and i). No signals were detected in a trachea section or the other extrapulmonary tissue sections. Many viral antigen-positive cells were detected in the earlier-stage DAD lesions before hyaline membrane formation (Figs. 3f, g, h, and i) rather than in the progressed lesions (Fig. 3j). The signals were found in alveolar epithelial cells, both type I and type II pneumocytes (Figs. 3b, d, g, and i). The influenza (A/H1N1dm) virus genomic RNA (minus-strand RNA) and mRNA (plus-strand RNA) were detected in the same lesion by the in situ hybridization AT-tailing CSA (ISH-AT-CSA) method using strand-specific oligonucleotide probes for the NP region of the influenza (A/H1N1pdm) virus (sense probe: 5′-gcaaggttcaacacttcccagaaggtctggtgccgcaggt-ATATATATATATATATATATAT-3′, anti-sense probe: 5′-acctgcgg caccagaccttctgggaagtgttgaaccttgc-ATATATATATATATATATAT AT-3′) (Figs. 4a and b) (8,9). This revealed that the virus had replicated in the alveolar epithelial cells. No signals were detected using an irrelevant probe as a negative control (Fig. 4c).

To characterize the virus-infected cells, confocal laser scanning microscopy was used to visualize double immunofluorescence staining for InfA-NP and for the cell type-specific marker proteins EMA (epithelial cells), SP-D (type II pneumocytes), cytokeratin AE1/AE3 (epithelial cells), CD68 (macrophages) and CD34 (endothelial cells) as previously described (10). Alexa Fluor 568-conjugated anti-mouse or anti-rabbit IgG (Molecular Probes, Eugene, Oreg., USA) and Alexa Fluor 488-conjugated anti-rabbit or anti-mouse IgG (Molecular Probes) were used as secondary antibodies. Almost all InfA-NP signals were detected in epithelial (EMA-positive) cells (Fig. 4d). They were also detected in SP-D-positive cells, suggesting type II pneumocytese (Fig. 4e). A few were detected in AE1/AE3-positive bronchial epithelial cells. None were detected in CD68-positive macrophages or CD34-positive endothelial cells (data not shown).

The influenza A virus binds to receptors containing terminal sialic acids linked to galactose on cell surface glycoproteins by a 2-3 linkage (SAα2-3Gal) and/or by a 2-6 linkage (SAα2-6Gal) (11). Swine influenza HA binds to both SAα2-6Gal and SAα2-3Gal (12). In the human respiratory organs, putative SAα2-6Gal receptors were mainly expressed in the epithelium of the upper respiratory tract and SAα2-3Gal receptors were expressed in the epithelium of the lower respiratory tract (data not shown). The sections were incubated

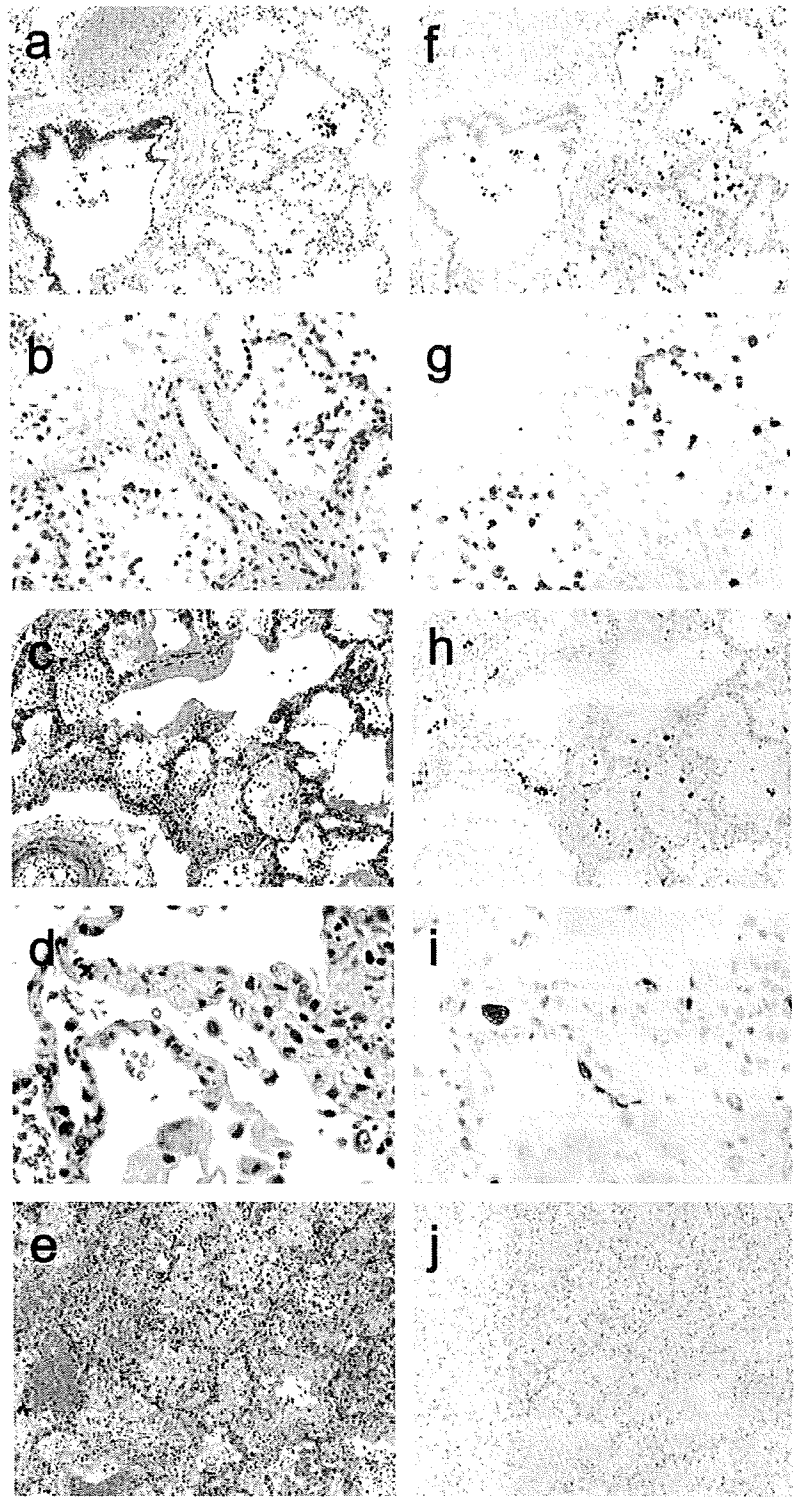

Fig. 3. Hematoxylin and eosin staining (a, b, c, d, and e) and immunohistochemistry for influenza A nucleoprotein (InfA-NP) (f, g, h, i, and j). Intra-alveolar edema with liquid, fibrin, erythrocytes and desquamated epithelial cells in alveolar spaces, hyperplasia of type II pneumocytes, and hemosiderin-laden macrophages (heart failure cells) were generally observed. (a) Regenerative hyperplasia and desquamation of the pseudostratified columnar epithelium of the bronchi were observed. (b, c, d) Early exudative-stage diffuse alveolar damage (DAD) with hyaline membrane formation. (e) More progressed proliferative-stage DAD were shown. (f, g, h, and i) A lot of viral antigen-positive cells were detected in the earlier-exudative stage DAD lesions before hyaline membranes formation. (i) The signals were also found in alveolar type I pneumocytes. (j) Few viral antigen-positive cells were detected in the progressed lesion. Original magnification, ×100 (a, c, e, f, h, and j), ×200 (b, g), ×400 (d, i).

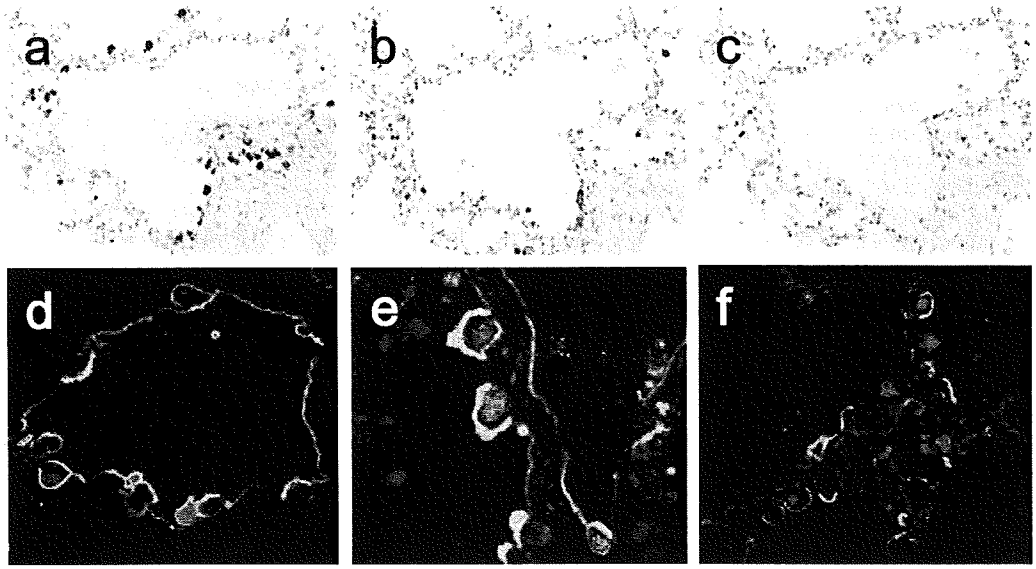

Fig. 4. The detections of influenza (A/H1N1pdm) virus-RNA using in situ hybridization AT-tailing-CSA method. (a) The influenza (A/H1N1pdm) virus genomic-RNA detected using a sense-probe. (b) The influenza (A/H1N1pdm) virus-mRNA detected using an anti-sense probe. (c) No signals were detected using an irrelevant probe. Original magnification, ×200. Double immunofluorescence staining. (d) Influenza virus A nucleoprotein (InfA-NP) (red) and EMA for epithelial cells (green) were co-localized. (e) InfA-NP (red) and SP-D for type II pneumocytes (green) were co-localized. (f) InfA-NP (red) were detected in the cells expressing sialic acids linked to galactose by a 2-3 linkage (SAα2-3Gal) (green). Original magnification, ×400.

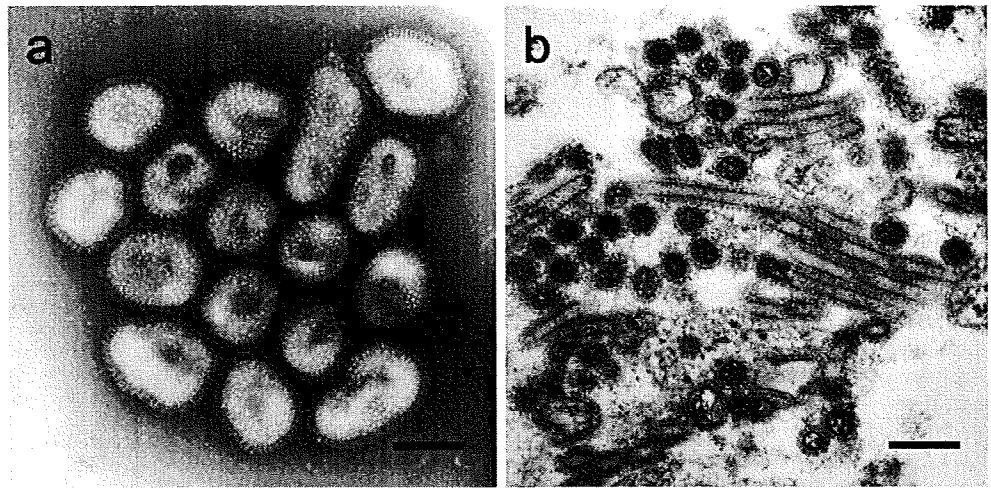

Fig. 5. Electron microscopy. (a) The negative staining feature of isolated influenza (A/H1N1pdm) virus particles in the culture supernatant. Scale bar, 100 nm. (b) The influenza (A/H1N1pdm) viral particles in filamentous forms in the lung sections. Scale bar, 200 nm.

with biotinylated-*Maackia amurensis* lectin II (MAA-II) (Vector Laboratories, Burlingame, Calif., USA) to detect SAα2-3Gal and with biotinylated-*Sambucus nigra* lectin I (SNA-I) (EY Laboratories, San Mateo, Calif., USA) to detect SAα2-6Gal. They were then incubated with Fluor 488-conjugated streptavidin (Molecular Probes). Double fluorescence staining and visualization with a confocal laser scanning microscope revealed that some infA-NP-positive cells expressed SAα2-3Gal on the cell surface (Fig. 4f), suggesting that A/H1N1pdm HA is able to bind to SAα2-3Gal receptors and to infect type II pneumocytes. Because few infA-NP are detected in bronchial epithelial cells on day 8 in this case, it was difficult to confirm that A/H1N1pdm HA was able to bind to SAα2-6Gal receptors, which are abundant on the surface of bronchial epithelial cells.

To examine the copy numbers of the influenza (A/H1N1pdm) virus, RNAs extracted from 4 paraffin-embedded sections (5 μm × 3) (left upper lung, left lower lung, left bronchus, middle trachea) were identified by quantitative real-time RT-PCR using an Mx3005P system (Stratagene, La Jolla, Calif., USA), which amplified a segment within the HA region of the A/H1N1pdm virus-RNA (13). The amount of human beta-actin mRNA in the DNase-treated RNA extracted from each section was also determined as an internal reference gene to provide a normalization factor for the amount of RNA isolated from a specimen (14). To amplify A/H1N1pdm-HA, forward (swH1N1-HA-F: 5′-CCCCATTGCA TTTGGGTAAA-3′) and reverse (swH1N1-HA-R: 5′-TGGA GAGTGATTCACACTGGAT-3′) primers were used with a labeled probe 5′-(FAM)AACATTGCTGGCTGGATCCTG

GGA(TAMRA)-3′. Real-time RT-PCR revealed 2.37×10^5 copies of A/H1N1pdm-RNA and 4.92×10^5 copies of beta-actin mRNA in the left lower lung section. The beta-actin mRNA copy number was 1,500 copies/cell (unpublished data). Therefore the influenza (A/H1N1pdm) virus-RNA copy number was calculated as 723 copies/cell in the left lower lung section. Similarly, it was calculated as 10 copies/cell in the left upper lung section, 2 copies/cell in the left bronchus and less than 1 copy/cell in the middle trachea. The differences in the copy numbers of influenza (A/H1N1pdm) virus-RNA among the sections were consistent with the differences in the numbers of InfA-NP-antigen-positive cells detected by immunohistochemistry.

A/H1N1pdm virus was isolated by inoculating 20% (w/v) homogenates of the autopsy lung tissue to Madin-Darby canine kidney (MDCK) cells in the presence of trypsin. The culture supernatants were harvested on the 3rd day post-inoculation as a stock virus. The virus titer, which was expressed as 50% of the tissue culture infectious dose ($TCID_{50}$)/ml on MDCK cells, was 7.5×10^5 $TCID_{50}$/ml. The whole sequence of the influenza virus proliferated in the lung was determined directly using an Illumina Genome Analyzer II (Illumina, San Diego, Calif., USA) and indirectly using the isolated strain. Both sequences mostly coincided with that of A/H1N1pdm. The former sequence was named A/Nagano/RC1-L/2009(H1N1) and the latter one was named A/Nagano/RC1/2009(H1N1). The negative staining feature of isolated A/H1N1pdm virus particles in the culture supernatant by electron microscopy (EM) is shown in Fig. 5a. In the lung tissue processed routinely for EM (15), outside of type II alveolar epithelial cells, influenza virus particles in filamentous rather than spherical forms were found (Fig. 5b).

The concentration of various cytokines/chemokines in the serum on day 5 and the autopsied lung tissue were measured by using a Human Cytokine 25-plex (BioSource International, Inc., Carmarillo, Calif., USA) and Luminex100TM (Luminex Co., Austin, Texas, USA) as described previously (16). IL-2R, IL-6, IL-8, IL-10, IFN-α, MCP-1, and MIG levels were elevated both in the serum on day 5 before corticosteroid treatment and the autopsy lung tissue on day 8. In addition to these data, an increase of IP-10 was observed in the serum and an increase of IFN-γ was detected in the lung tissue.

The patient had multiple risk factors for severe complications of influenza (A/H1N1pdm) virus infection, suggesting that he died of respiratory failure due to severe pulmonary edema caused by both chronic heart failure and influenza pneumonia. The lung sections showed very early exudative-stage DAD before hyaline membrane formation. Unexpectedly, a high level of proliferation of influenza (A/H1N1pdm) virus was detected in alveolar epithelial cells by immunohistochemistry, as shown in Fig. 3. We were able to detect this early stage of the disease even in the autopsied lung sections. This case provide clues to the pathogenesis of influenza pneumonia and suggests what occurs in the lungs after influenza (A/H1N1pdm) virus infection.

ACKNOWLEDGMENTS

This study was supported by the Health and Labour Sciences Research Grants on Emerging and Re-emerging Infectious Diseases (to TS and NN, No. H20-Shinko-Ippan-006 and H19-Shinko-Ippan-005) from the Ministry of Health, Labour and Welfare of Japan.

We thank Drs. Takahiro Tsuji, Naoko Iwata, and Yuko Sasaki for their technical assistance, and Dr. Toshio Kumasaka for valuable discussions.

REFERENCES

1. Centers for Disease, Control and Prevention (2009): Intensive-care patients with severe novel influenza A(H1N1) virus infection—Michigan. Morbid. Mortal. Wkly. Rep., 58, 749–752.
2. Centers for Disease, Control and Prevention (2009): Neurologic complications associated with novel influenza A (H1N1) virus infection in children—Dallas, Texas. Morbid. Mortal. Wkly. Rep., 58, 773–778.
3. Perez-Padilla, R., de la Rosa-Zamboni, D., Ponce de Leon, S., et al. (2009): Pneumonia and respiratory failure from swine-origin influenza A (H1N1) in Mexico. N. Engl. J. Med., 361, 680–689.
4. Ministry of Health, Labour and Welfare, Japan: Situation of H1N1 in Japan. Online at <http://www.mhlw.go.jp/za/0806/c17/c17.html>.
5. Mauda, T., Hajjar, L.A., Callegari, G.D., et al. (2010): Lung pathology in fatal novel human influenza A (H1N1) infection. Am. J. Respir. Crit. Care Med., 181, 72–79.
6. Gill, J.R., Sheng, Z.M., Ely., S.F., et al. (2010): Pulmonary pathologic findings of fatal 2009 pandemic influenza A/H1N1 viral infections. Arch. Pathol. Lab. Med., 134 (published on line).
7. Chen, Z., Sahashi, Y., Matsuo, K., et al. (1998): Comparison of the ability of viral protein-expressing plasmid DNAs to protect against influenza. Vaccine, 16, 1544–1549.
8. Nakajima, N., Ionescu, P., Sato, Y., et al. (2003): In situ hybridization AT-tailing with catalyzed signal amplification for sensitive and specific in situ detection of human immunodeficiency virus-1 mRNA in formalin-fixed and paraffin-embedded tissues. Am. J. Pathol., 162, 381–389.
9. Nakajima, N., Asahi-Ozaki, Y., Nagata, N., et al. (2003): SARS coronavirus-infected cells in lung detected by new in situ hybridization technique. Jpn. J. Infect. Dis., 56, 139–141.
10. Liem, N.T., Nakajima, N., Phat, L.P., et al. (2008): H5N1-infected cells in lung with diffuse alveolar damage in exudative phase from a fatal case in Vietnam. Jpn. J. Infect. Dis., 61, 157–160.
11. Shinya, K., Ebina, M., Ono, M., et al. (2006): Avian flu: influenza receptors in the human airway. Nature, 440, 435–436.
12. Gambaryan, A.S., Tuzikov, A.B., Piskarev, V.E., et al. (1997): Specification of receptor-binding phenotypes of influenza virus isolates from different hosts using synthetic sialyglycopolymers: non-egg-adapted human H1 and H3 influenza A and influenza B viruses share a common high binding affinity for 6′-sialyl (*N*-acetyllactosamine). Virology, 232, 345–350.
13. Katano, H., Ito, H., Suzuki, Y., et al. (2009): Detection of Merkel cell polyomavirus in Merkel cell carcinoma and Kaposi's sarcoma. J. Med. Virol., 81, 1951–1958.
14. Kuramochi, H., Hayashi, K., Uchida, K., et al. (2006): Vascular endothelial growth factor messenger RNA expression level is preserved in liver metastases compared with corresponding primary colorectal cancer. Clin. Cancer Res., 12, 29–33.
15. Tobiume, M., Sato, Y., Katano, H., et al. (2009): Rabies virus dissemination in neural tissues of autopsy cases due to rabies imported into Japan from Philippines: immunohistochemistry. Pathol. Int., 59, 555–566.
16. Nagata, N., Iwata, N., Hasegawa, H., et al. (2008): Mouse-passaged severe acute respiratory syndrome-associated coronavirus leads to lethal pulmonary edema and diffuse alveolar damage in adult but not young mice. Am. J. Pathol., 172, 1625–1637.

Jpn. J. Infect. Dis., 63, 72-74, 2010

Short Communication

Sudden Death of a Patient with Pandemic Influenza (A/H1N1pdm) Virus Infection by Acute Respiratory Distress Syndrome

Akihiro Takiyama[1], Lei Wang[1], Mishie Tanino[1], Taichi Kimura[1], Naoki Kawagishi[5], Yasuyuki Kunieda[5], Harutaka Katano[3], Noriko Nakajima[3], Hideki Hasegawa[3,4], Tomoyuki Takagi[5], Hiroshi Nishihara[2], Tetsutaro Sata[3], and Shinya Tanaka[1,2]*

[1]Laboratory of Cancer Research, Department of Pathology and [2]Department of Translational Pathology, Hokkaido University Graduate School of Medicine, Sapporo 060-8638; [3]Department of Pathology and [4]Influenza Virus Research Center, National Institute of Infectious Diseases, Tokyo 162-8640; and [5]Wakkanai Municipal Hospital, Wakkanai 097-8555, Japan

(Received December 22, 2009. Accepted January 5, 2010)

SUMMARY: We describe an autopsy case of a patient with pandemic influenza (A/H1N1pdm) virus infection in Japan, who developed rapidly progressive viral pneumonia exhibiting diffuse alveolar damage. A 41-year-old female visited our hospital with a fever of 38.7°C. She was a public health nurse with no underlying disease and had had contact with a group of elementary school students who had been infected with the influenza (A/H1N1pdm) virus 1 week earlier. She was prescribed oseltamivir and returned to the hotel where she was staying alone. The next day, she was found dead in her hotel room. At autopsy, both lungs were voluminous and microscopic examination revealed acute-stage, severe diffuse alveolar damage with remarkable mononuclear cell infiltration and hyaline membrane formation in the lungs. CD8-positive T lymphocytes were dominantly observed. Immunohistochemically, influenza A viral protein was confirmed in the damaged type II pneumocytes and also in the infiltrated macrophages. Real-time RT-PCR analysis of both pre- and post-mortem pharyngeal swabs confirmed a novel influenza (A/H1N1pdm) virus infection. This is the second autopsy case of influenza (A/H1N1pdm) virus infection in Japan, and the findings indicated that the patient died due to an exceptionally rapid progression of viral pneumonia. This case indicates that patients with influenza (A/H1N1pdm) virus infection should be carefully monitor for acute respiratory distress syndrome.

In March 2009, a novel swine-derived influenza (A/H1N1pdm) virus was identified in California and Mexico (1,2). On June 11, 2009, the World Health Organization declared that infections caused by the new strain had reached pandemic proportion. On December 6, 2009, it was reported that 9,596 deaths had been associated with the pandemic worldwide (3), and on December 28, 2009, it was reported that 133 deaths had been linked to the virus in Japan (4). Here, we describe the second autopsy case of a patient with influenza (A/H1N1pdm) virus infection in Japan, which was characterized by rapidly progressive viral pneumonia exhibiting diffuse alveolar damage.

A 41-year-old female visited our hospital with a fever of 38.7°C. She was a public health nurse with no underlying disease and had had contact with a group of elementary school students who had been infected with the influenza (A/H1N1pdm) virus twice, once 5 days and once 8 days before presentation at our hospital. She had experienced a mild cough several days ago, but no other symptoms were observed. Oseltamivir was prescribed and she went back to her hotel alone. The next day, she was found dead in her hotel room; she had not yet taken any oseltamivir tablets.

At autopsy, she was found to have obesity, with a BMI of 30.2 (BL, 149 cm; BW, 67.3 kg; waist, 88 cm). The bilateral lungs were voluminous (left, 560 g; right, 550 g; Figs. 1a and b), but there was little pleural effusion. Microscopically, prominent mononuclear cell infiltration with fibrinous exudates was observed throughout the entire lung by H&E staining (Figs. 1c, d, e, and f). Hyaline membrane formation was found in a part of the lung, suggesting diffuse alveolar damage (Fig. 1e). Hyperplasia of the alveolar pneumocytes was not evident. Necrotizing bronchitis and bronchiolitis were prominently observed (Fig. 1g). Degenerative changes in the epithelial cells of the bronchial and bronchiolar mucosa and the bronchial glands were seen (Fig. 1g). Thrombosis of the capillaries and arteries was not evident (Fig. 1h). Immunohistochemically, the infiltrating lymphocytes were mostly positive for CD4 and CD8, and the CD4/CD8 ratio was lower than 1.0 (Figs. 1i and j).

To analyze the distribution of the influenza (A/H1N1pdm) virus antigen, 10% formalin-fixed paraffin-embedded tissue sections were immunostained by an avidin-biotin complex immunoperoxidase method (LSAB2 kit/HRP/DAB; Dako Cytomation, Copenhagen, Denmark) using a mouse monoclonal antibody against influenza A nucleoprotein (InfA-NP) (5). Positivity for InfA-NP was observed in the damaged cells, which were morphologically consistent with epithelial cells and macrophages (Fig. 2).

To characterize the virus-infected cells, a confocal laser scanning microscope was used to visualize double immunofluorescence staining for InfA-NP and for the cell type-specific marker proteins EMA (epithelial cells) and CD68 (macrophages) as previously described (6). Alexa Fluor 568-conjugated anti-rabbit IgG (Molecular Probes, Eugene, Oreg., USA) and Alexa Fluor 488-conjugated anti-mouse IgG (Molecular Probes) were used as secondary antibodies for InfA-NP and

*Corresponding author: Mailing address: Laboratory of Cancer Research, Department of Pathology, Hokkaido University Graduate School of Medicine, N15W7, Kita-ku, Sapporo 060-8638, Japan. Tel: +81-11-706-5052, Fax: +81-11-706-5902, E-mail: tanaka@med.hokudai.ac.jp

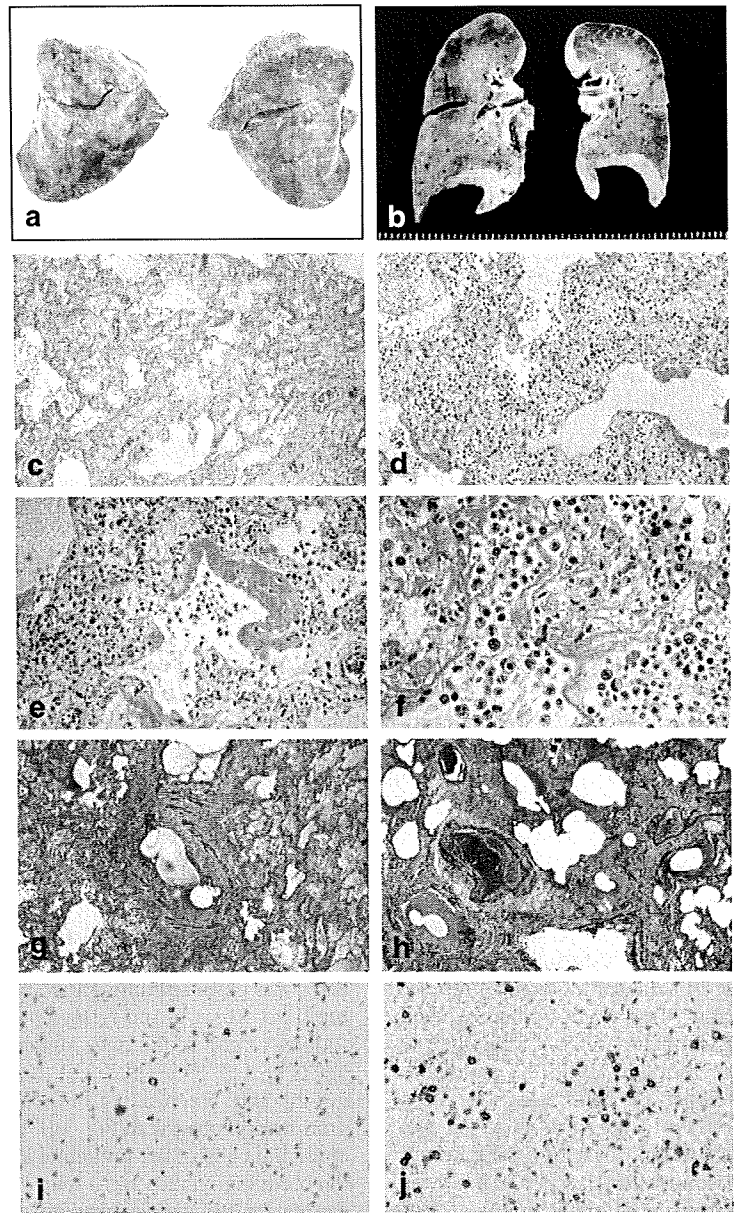

Fig. 1. Autopsy findings of the lung. (a and b) Gross appearance of bilateral lung and the sectioned surface. (c-f) Microscopic findings. Prominent mononuclear cell infiltration with fibrinous exudates was observed throughout the entire lung. Partially, hyaline membrane formation was prominent (e). (g) Necrotizing bronchitis and bronchiolitis were observed. (h) Elastica-Masson stain. Thrombosis of the capillaries and arteries was not evident. (i and j) Immunostaining for CD4 (i) and CD8 (j).

EMA/CD68, respectively. Double staining of epithelial membrane antigens and InfA-NP showed influenza A virus infection of the cytoplasm and/or nucleus of the damaged type II pneumocytes (Fig. 3a). In addition, combination staining with InfA-NP and CD68 revealed influenza virus infection in macrophages (Fig. 3b). Most of the tracheal epithelia were desquamated, only those of upper portion remained, and influenza (A/H1N1pdm) virus antigen was not detected in these areas. The liver showed fatty changes, mainly centrilobular. No pathognomonic findings were observed in other organs, including the brain (1,300 g) and the heart (430 g).

Real-time RT-PCR examination of both pre- and post-mortem pharyngeal swabs, performed by the Hokkaido Public Health Institute, confirmed the novel influenza (A/H1N1pdm) virus infection. Further analysis demonstrated the relatively lower copy number of infected virus in the lung tissue (data not shown).

Influenza (A/H1N1pdm) virus infection can cause acute respiratory distress syndrome (1,7,8). In the present case, a public health nurse was infected with influenza (A/H1N1pdm) virus and died of severe respiratory distress syndrome due to severe diffuse alveolar damage. She had no underlying disease except for obesity, which has been reported to confer an increased risk of death from influenza (A/H1N1pdm) virus (2). Alveolar involvement is unusual but such cases seem to have been common during the 1918–1919 pandemic (9). In the current case, immunohistochemical study clearly confirmed the influenza (A/H1N1pdm) virus infection of damaged type II pneumocytes. In consistent with our finding, Mauad et al. described 21 autopsy cases with confirmed novel influenza

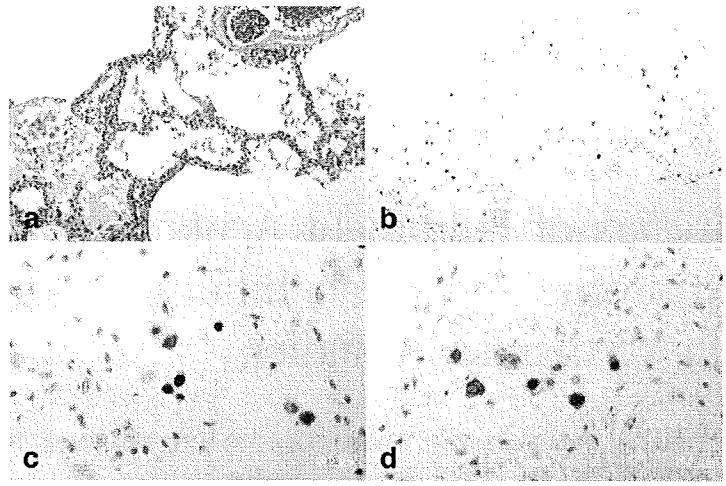

Fig. 2. Immunohistochemical analysis of influenza A virus nucleoprotein (InfA-NP). (a) H&E stain of the damaged lung. (b-d) Immuno-stain of InfA-NP. Nuclear and cytoplasmic positivities were observed in damaged and/or inflammatory cells.

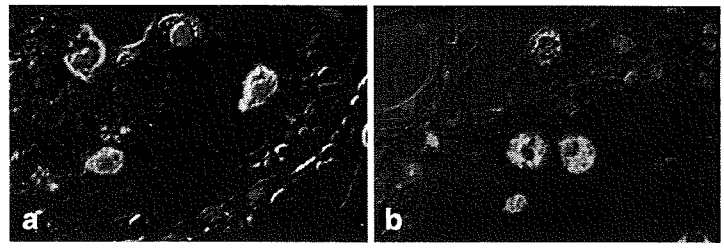

Fig. 3. Analysis of the infected cells. (a) Double staining of epithelial membrane antigen (green) and InfA-NP (red). Nuclear stain (blue). (b) Double staining of CD68 (green) and InfA-NP (red). Nuclear stain (blue).

(A/H1N1pdm) virus infection, and reported that diffuse alveolar damage was present in 20 individuals (10).

One of the significant features of this case was the remarkably rapid disease progression, with the patient dying less than 24 h after presentation. Viral overload leads to altered innate immune responses such as sustained TLR-3 activation, enhanced inflammation with high numbers of CD8-positive T lymphocytes, and local production of IFN-γ, all of which have been suggested to contribute to virally induced lung injury (11). In the present case, the cause of the diffuse alveolar damage was unknown, but an increase of CD8-positive T cells may have altered the immune response leading to lung injury. Therefore, when caring for the influenza (A/H1N1pdm) virus-infected patients, it is important to carefully exclude the possibility of severe acute distress syndrome, which can cause sudden death.

ACKNOWLEDGMENTS

We thank Kazuko Shimizu and Eiko Aoyanagi for the excellent pathological technique.

This work was supported by Grants-in-Aid for Scientific Research from the Ministry of Education, Culture, Sports, Science and Technology (MEXT) of Japan.

REFERENCES

1. Perez-Padilla, R., de la Rosa-Zamboni, D., Ponce de Leon, S., et al. (2009): Pneumonia and respiratory failure from swine-origin influenza A (H1N1) in Mexico. N. Engl. J. Med., 361, 680–689.
2. Echevarría-Zuno, S., Mejía-Aranguré, J.M., Mar-Obeso, A.J., et al. (2009): Infection and death from influenza A H1N1 virus in Mexico: a retrospective analysis. Lancet, published online Nov 12. DOI:10.1016/S0140–6736(09)61638–X.
3. World Health Organization: Pandemic (H1N1) 2009–update 78. 2009. Online at <http://www.who.int/csr/don/2009_12_11a/en/index.html>. Accessed 12 December 2009.
4. Ministry of Health, Labour and Welfare, Japan: http://www.mhlw.go.jp/bunya/kenkou/kekkaku-kansenshou04/rireki/091202-03.html, http://www.mhlw.go.jp/kinkyu/kenkou/influenza/houdou.html (in Japanese).
5. Chen, Z., Sahashi,Y., Matsuo, K., et al. (1998): Comparison of the ability of viral protein-expressing plasmid DNAs to protect against influenza. Vaccine, 16, 1544–1549.
6. Liem, N.T., Nakajima, N., Phat, L.P., et al. (2008): H5N1-infected cells in lung with diffuse alveolar damage in exudative phase from a fatal case in Vietnam. Jpn. J. Infect. Dis., 61, 157–160.
7. Chowell, G., Bertozzi, S.M., Colchero, M.A., et al. (2009): Severe respiratory disease concurrent with the circulation of H1N1 influenza. N. Engl. J. Med., 361, 674–679.
8. Novel Swine-Origin Influenza A (H1N1) Virus Investigation Team, Dawood, F.S., Jain, S., Finelli, L., et al. (2009): Emergence of a novel swine-origin influenza A (H1N1) virus in humans. N. Engl. J. Med., 360, 2605–2615.
9. Kobasa, D., Jones, S.M., Shinya, K., et al. (2007): Aberrant innate immune response in lethal infection of macaques with the 1918 influenza virus. Nature, 445, 319–323.
10. Mauad, T., Hajjar, L.A., Callegari, G.D., et al. (2009): Lung pathology in fatal novel human influenza A (H1N1) infection. Am. J. Respir. Crit. Care Med. Published on October 29, 2009 as doi:10.1164/rccm.200909–1420OC.
11. Zhao, M.Q., Amir, M.K., Rice, W.R., et al. (2001): Type II pneumocyte-CD8+ T-cell interactions. Relationship between target cell cytotoxicity and activation. Am. J. Respir. Cell Mol. Biol., 25, 362–369.

MAJOR ARTICLE

Risk Parameters of Fulminant Acute Respiratory Distress Syndrome and Avian Influenza (H5N1) Infection in Vietnamese Children

Shoji Kawachi,[1,3] San Thi Luong,[7] Mika Shigematsu,[2] Hiroyuki Furuya,[4] Thuy Thi Bich Phung,[7] Phuc Huu Phan,[7] Hiroyuki Nunoi,[5] Liem Thanh Nguyen,[7] and Kazuo Suzuki[1,6]

[1]Department of Immunology and [2]Infectious Disease Surveillance Center, National Institute of Infectious Diseases, and [3]Division of Anaesthesia, Surgical Operation Department, International Medical Center of Japan, Tokyo, [4]Basic Clinical Science and Public Health, Tokai University School of Medicine, Isehara, [5]Division of Pediatrics, Department of Reproductive and Developmental Medicine, Faculty of Medicine, University of Miyazaki, Miyazaki, and [6]Inflammation Program, Department of Immunology, Chiba University Graduate School of Medicine, Chiba, Japan; and [7]National Hospital of Pediatrics, Hanoi, Vietnam

A clinical picture of patients with acute respiratory distress syndrome (ARDS) induced by highly pathogenic avian influenza A (H5N1) has been reported. We reviewed 37 sets of clinical data for pediatric patients with ARDS at the National Hospital of Pediatrics (Hanoi, Vietnam); 12 patients with H5N1-positive and 25 with H5N1-negative ARDS were enrolled. The H5N1-negative patients had a clinical picture and mortality rate similar to that for the pediatric ARDS patients. However, the H5N1-positive patients had ARDS with normal ventilation capacity at the time of hospital admission, then rapidly proceeded to severe respiratory failure. The survival probability and days until final outcome in groups of H5N1-positive (n = 12) vs. H5N1-negative (n = 25) patients were 17% versus 52% and 12.3 ± 5.7 days (median, 11 days) versus 21.5 ± 13.8 days (median, 22 days), respectively. Our observations clarified the clinical picture of H5N1-induced fulminant ARDS and also confirmed that relatively older age (~6 years of age), high fever at onset, and leukopenia and/or thrombocytopenia at the time of hospital admission are risk parameters for H5N1-induced fulminant ARDS.

Highly pathogenic avian influenza A (H5N1) came to the attention of the international scientific community for the first time in 1997 [1, 2]. The current global spread of human infection by this subtype started in 2003 in Hong Kong [2, 3], during the global outbreak of severe acute respiratory syndrome [4, 5]. Vietnam reported the first human case of H5N1 infection in January 2004 [6] and a suspected human-to-human transmission family cluster in the following months [7]. Since then, many clinical case reports have been reported from several countries, such as Thailand, Indonesia, and Vietnam [8–14]. However, it is still difficult to detect most infection at first examination without a clear history of patient contact with sick poultry.

The fatality rate associated with pediatric acute respiratory distress syndrome (ARDS) has decreased during recent decades because of advances in medical treatment, especially respiratory management as a lung-protective therapy [15]. However, the majority of patients with H5N1 subtype influenza virus infection experienced or presented ARDS during their clinical courses, often followed by a serious outcome. The histopathology of these cases demonstrated diffuse alveolar damage in the lung, which also suggests ARDS as a clinical condition of the respiratory system [16–18]. Because of the significant possibility that H5N1 subtype influenza will the source of the next pandemic influenza strain [19, 20], the pathophysiology of the clinical course of H5N1

Received 27 February 2009; accepted 8 April 2009; electronically published 9 July 2009.

Potential conflicts of interest: none reported.

Financial support: Research-in Aid Grant from the Ministry of Health, Labour, and Welfare of Japan (H19-Shinko-Ippan-005).

Reprints or correspondence: Kazuo Suzuki, Ph.D., Inflammation Program, Dept. of Immunology, Chiba University Graduate School of Medicine, Chiba, Japan, Inohana 1-8-1, Chuo-ku, Chiba, 260-8670, Japan (ksuzuki@faculty.chiba-u.jp).

The Journal of Infectious Diseases 2009;200:510–15

0022-1899/2009/20004-0005$15.00

DOI: 10.1086/605034

Table 1. Clinical Features of H5N1-Positive and H5N1-Negative Patients

Feature	H5N1-positive patients (n = 12) Mean value ± SD	Median value	H5N1-negative patients (n = 25) Mean value ± SD	Median value	P
Age, year	6.7 ± 3.9	6	1.2 ± 2.9	0.3	<.001
pH	7.46 ± 0.07	7.49	7.29 ± 0.17	7.32	<.001
PaO_2, mmHg	61.4 ± 59.3	41.9	58.9 ± 23.8	58.6	.253
$PaCO_2$, mmHg	33.2 ± 12.4	32.5	47.5 ± 18.1	41.3	.009
FiO_2	0.81 ± 0.28	1	0.82 ± 0.27	1	.987
Body temperature at onset, °C	39.1 ± 0.4	39	37.7 ± 1	37.8	<.001
WBC count, cells/mm^3[a]	2863.6 ± 1545	2300	13,376 ± 9478	11,000	<.001
Platelet count × 10^3, cells/mm^3[a]	123.5 ± 52.3	125	366 ± 179.5	374	<.001
AST level, IU/L[a]	1723 ± 2784	724	259 ± 653	105	<.001
ALT level, IU/L[a]	628 ± 1042	248	221 ± 845	40	<.001

Variable	H5N1-positive patients, no. (%) of patients (n = 12)	H5N1-negative patients, no. (%) of patients (n = 25)	P
Prognosis			
Alive	2 (16.7)	13 (52.0)	.091
Dead	10 (83.3)	12 (48.0)	
Sex			
Male	8 (66.7)	8 (32.0)	.046
Female	4 (33.3)	17 (68.0)	
Multiple organ failure			
Yes	1 (8.3)	18 (72.0)	<.001
No	11 (91.7)	7 (28.0)	

NOTE. P values <.05 indicate statistically significant differences between H5N1-positive and H5N1-negative groups. ALT, alanine aminotransferase; AST, aspartate aminotransferase; SD, standard deviation; WBC, white blood cell.

[a] WBC and platelet counts were available for only 11 H5N1-positive patients, and AST and ALT levels were available for only 7 H5N1-positive patients and 23 H5N1-negative patients.

influenza virus infection and the identification of the key objective clinical data are crucial pieces of information that will help physicians provide timely and adequate treatment.

In the present study, we reviewed the clinical data from pediatric ARDS cases to identify distinctive findings of cases of H5N1 subtype influenza virus infection among Vietnamese children. This work was performed in close collaboration with the National Hospital of Pediatrics (NHP) in Hanoi and was supported by the Ministry of Health, Labour, and Welfare in Japan and the Ministry of Health in Vietnam.

MATERIALS AND METHODS

Data source. Clinical and laboratory data for pediatric patients (aged >1 month) with severe illness examined at the NHP from December 2003 through June 2008 were analyzed. Patients examined prior to 2007 were enrolled in the study retrospectively by hospital record review and were followed prospectively after hospital admission. The diagnosis of ARDS was made according to international standards [21], which involve acute onset; PaO_2/FiO_2 ratio (P/F ratio) <200, independent of controlled mechanical ventilation; and bilateral infiltration observed on chest radiography without left heart failure or with pulmonary artery wedge pressure <18 mmHg. We enrolled patients with severe ARDS whose P/F ratios were <100 during their clinical courses. H5N1 infection was confirmed with throat and/or nasal swabs tested by reverse-transcriptase polymerase chain reaction at the hospital laboratory or at the National Institute of Hygiene Epidemiology (Hanoi). The study was reviewed by the ethical committee of the International Medical Center Japan in 2007, and the design was approved on 28 September 2007.

Statistical methods. Fisher's exact test was employed for bivariate analysis of categorical data. The nonparametric Mann-Whitney test was used for 2-group comparisons of continuous data. Survival curves and rates were calculated by the Kaplan-Meier method. The log-rank (Mantel-Cox) test was used for the comparison of 2 survival curves. All statistical analyses were performed with SPSS, version 14.0 (SPSS).

RESULTS

Thirty-nine patients with ARDS who met the inclusion criteria visited the hospital during the study period, but 2 were excluded

Table 2. Summary of All Clinical Data

Patient	Sex	Age, years	Duration,[a] days	Prognosis		BT at onset, °C	Blood pH	Respiratory parameters				Liver function levels, IU/L		Blood counts[b]			Cause of ARDS
				Death	MOF			PaO_2, mmHg	$PaCO_2$, mmHg	P/F	Lowest P/F	AST	ALT	WBC	RBC	PLT	
H5N1 positive (n = 12)																	
1	F	12	7	Yes	Yes	39.5	7.48	29.1	30.7	29	29	NT	NT	2100	4510	45	Pneumonia (H5N1)
2	M	5	16	Yes	No	39.0	7.49	70.3	35.0	70	35	NT	NT	3400	4380	174	Pneumonia (H5N1)
3	M	10	11	Yes	No	39.5	7.51	33.5	28.1	84	24	NT	NT	2800	3750	143	Pneumonia (H5N1)
4	F	5	7	Yes	No	39.5	7.34	29.1	54.1	29	29	NT	NT	1100	3980	91	Pneumonia (H5N1)
5	M	4	15	Yes	No	39.5	7.5	40.9	26.1	41	36	NT	NT	2300	4190	150	Pneumonia (H5N1)
6	F	1	6	Yes	No	38.5	7.41	76.1	26.2	190	34	1121	484	NT	NT	NT	Pneumonia (H5N1)
7	M	1.3	9	Yes	No	39.0	7.52	243.0	9.3	607	65	8010	2972	1400	2190	31	Pneumonia (H5N1)
8	M	11	11	Yes	No	39.0	7.54	34.0	22.0	34	34	801	217	4800	4500	125	Pneumonia (H5N1)
9	F	9	26	No	No	39.5	7.47	42.8	34.2	43	43	312	248	6300	3970	122	Pneumonia (H5N1)
10	M	4	12	Yes	No	38.5	7.44	31.4	43.1	31	18	583	89	2300	4220	154	Pneumonia (H5N1)
11	M	7	18	No	No	38.5	7.49	58.0	41.0	116	97	511	105	3300	398	116	Pneumonia (H5N1)
12	M	11	10	No	No	39.5	7.55	52.0	29.6	52	49	724	282	1700	4530	207	Pneumonia (H5N1)
H5N1 negative (n = 25)																	
13	F	4	2	Yes	Yes	38.8	7.33	58.6	32.4	59	52	77	49.5	9300	2990	83	Pneumonia
14	M	0.2	23	No	Yes	34.3	7.35	34.5	41.3	35	31	142	67	3250	4030	57	Pneumonia
15	M	0.2	53	No	No	37.4	7.37	74.5	29.6	186	50	NT	NT	29200	4250	547	Unknown
16	F	3	29	No	Yes	38.5	7.19	25.0	50.0	25	25	55	36	4000	3030	37	Pneumonia
17	F	3	19	Yes	Yes	39.0	7.31	34.5	40.5	35	35	284	55	1600	3910	352	Pneumonia
18	M	0.4	2	Yes	Yes	38.5	7.32	108.0	28.2	108	47	120	31	4200	NT	332	Pneumonia
19	F	0.33	8	Yes	Yes	38.5	7.30	108.4	31.4	108	38	126	31	9500	3680	374	Pneumonia
20	F	0.18	10	Yes	Yes	37.2	7.29	67.0	43.0	67	31	105	37	19100	3690	448	Pneumonia (rhinovirus)
21	F	0.18	13	No	Yes	38.5	7.37	63.0	56.0	63	33	79	16	4200	3910	403	Pneumonia (rhinovirus)
22	F	0.18	6	Yes	Yes	37.5	7.31	24.0	56.5	24	24	77	44	23900	3640	534	Pneumonia (adenovirus)
23	F	0.25	8	Yes	Yes	38.0	7.23	42.7	75.7	43	26	287	51	16900	3450	176	Pneumonia (rhinovirus)
24	F	0.18	22	Yes	Yes	36.0	7.15	25.7	55.1	26	26	219	69	11000	3980	442	Pneumonia (rhinovirus)
25	F	0.25	5	Yes	Yes	37.8	6.61	75.6	113.6	76	76	196	40	14800	4010	590	Pneumonia
26	M	0.25	38	No	Yes	38.5	7.32	48.4	37.0	121	21	78	36	19000	4660	430	Pneumonia (bacterial)
27	F	14	12	No	Yes	37.5	7.45	95.1	37.0	95	95	3235	4097	28000	3510	278	Pneumonia
28	M	0.33	19	No	No	37.2	7.19	43.0	59.0	43	43	246	50	8600	3360	342	Pneumonia
29	M	0.25	36	No	Yes	36.9	7.32	39.0	40.0	98	49	83	25	1950	3200	497	Unknown
30	F	0.2	14	No	No	37.5	7.39	88.6	38.0	89	89	36	108	5300	5180	322	Pneumonia (bacterial)
31	F	0.12	35	No	Yes	37.2	7.41	61.0	41.0	153	55	118	52	13700	8480	592	Pneumonia
32	F	0.33	44	No	No	37.5	7.15	48.0	45.0	48	30	NT	NT	8800	4480	58	Pneumonia
33	F	0.2	35	No	Yes	38.5	7.30	70.0	31.0	175	49	99	38	28400	4290	532	Pneumonia
34	F	0.2	35	No	No	36.5	7.22	61.0	38.4	153	66	71	59	11400	3680	330	Pneumonia
35	M	0.25	22	Yes	Yes	38.0	7.47	58.0	63.0	73	22	46	14.6	10800	4140	508	Pneumonia (adenovirus)
36	F	0.2	23	Yes	No	38.6	7.36	65.0	50.0	65	27	111	27	12000	3440	233	Pneumonia
37	M	0.2	24	No	No	38.5	7.42	55.0	54.0	138	47	65	38	35500	3540	654	Unknown

NOTE. ALT, alanine aminotransferase; ARDS, acute respiratory distress syndrome; AST, aspartate aminotransferase; BT, body temperature; MOF, multiple organ failure; NT, not tested; P/F PaO_2/FiO_2 ratio; PLT, platelet; RBC, red blood cell; WBC, white blood cell.

[a] The duration represents the time from onset of illness to death or hospital discharge.

[b] WBC and RBC counts are cells/mm^3; PLT counts are 10^3 cells/mm^3.

because of insufficient medical data. Twelve of 37 patients were shown to be positive for H5N1 influenza by polymerase chain reaction performed in the laboratory of the NHP (table 1).

Most patients in the H5N1-positive group experienced rapid deterioration of ARDS and died of respiratory failure even with proper medical care. Although 3 patients had thrombocytopenia (patients 1, 4, and 7) and 7 (patients 6–12) had increased serum aminotransferase levels (table 2), multiple organ failure was not followed by pathological investigation for H5N1-positive patients (data not shown).

The P/F ratio of all patients enrolled in this study was <100 during their clinical courses. However, $PaCO_2$ level at hospital admission was lower among H5N1-positive than among the H5N1-negative patients, illustrating that ventilation capacity was higher in the H5N1-positive group, compared with the H5N1-negative group. These clinical features of ARDS in the H5N1-negative group made us wonder why ARDS in the H5N1-positive group was not more severe than that in the H5N1-negative group on hospital admission. The survival probability and days until final outcome (± standard deviation) among H5N1-positive (n = 12) and H5N1-negative (n = 25) patients were 17% and 52% and 12.3 ± 5.7 days (median, 11 days) and 21.5 ± 13.8 days (median, 22 days), respectively, demonstrating that the survival probability in the H5N1-positive group was significantly lower than that in the H5N1-negative group (P = .022, by log-rank test; P = .038, by Tarone-Ware test) (figure 1). These observations are the first step toward examining the clinical data for the H5N1-positive patients, which we designated as having fulminant ARDS.

As summarized in table 1, leukopenia and thrombocytopenia were observed in the H5N1-positive group, but leukophilia and normal-range thrombocyte levels were observed in the H5N1-negative group. Serum aspartate aminotransferase and alanine aminotransferase levels were also increased in the H5N1-positive but not the H5N1-negative group. Clinically, body temperature at illness onset in the H5N1-positive group was significantly higher than that in the negative group. We observed differences in clinical features between the H5N1-positive and H5N1-negative groups; we also analyzed differences with regard to sex, age distribution, and prognosis between these groups. The number of male patients in the H5N1-positive group was significantly higher than that in the H5N1-negative group, and H5N1-positive patients were significantly older than those in the H5N1-negative group. The mean time from illness onset until death (± standard deviation) was 10.4 ± 3.3 days (median, 10.5 days) in H5N1-positive group (n = 10) and 11.7 ± 3.3 days (median, 9 days) in H5N1-negative group (n = 12), and the mean time until hospital discharge (recovery) was 26 ± 18 days (median, 22 days) in the H5N1-positive group (n = 2) and 30.5 ± 11.8 days (median, 35 days) in the H5N1-negative group (n = 13). No significant differences were observed between groups with regard to time from illness onset to death.

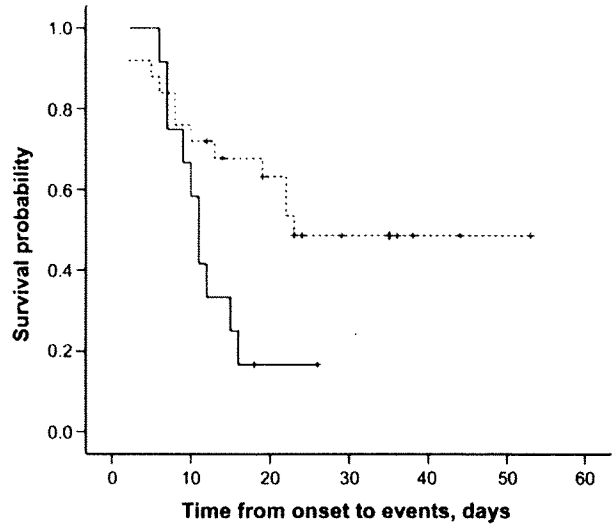

Figure 1. Survival probability for H5N1-positive (*solid line*) and H5N1-negative (*dashed line*) patients. For differences between 2 groups, P = .022 (by log-rank test) and P = .038 (Tarone-Ware test). The duration (± standard deviation) with disease until final outcome was 12.3 ± 5.7 days (median, 11 days) for the H5N1-positive group and 21.5 ± 13.8 days (median, 22 days) for the H5N1-negative group.

DISCUSSION

H5N1-infected patients were significantly older than patients in the comparator group. To our knowledge, the mortality rate by age has not been discussed precisely for pediatric patients with ARDS; Flori et al [22] collectively discussed age and mortality in their analysis of 328 patients with ARDS who were aged between 36 weeks (corrected gestational age) and 18 years, and the mortality rate among patients with a P/F ratio <100 was ~35%. The observed significant difference in mortality rate by age could prove that relatively older age (6.7 ± 3.9 vs 1.2 ± 2.9 years) is one of the risk factors for H5N1 infection.

ARDS frequently results in a lethal outcome attributable not only to respiratory failure but also to multiple organ failure [15, 23, 24]. Our study confirmed that survival of patients with ARDS aged <16 years is drastically improved by medical care, but that these patients die of respiratory failure and multiple organ failure [14]. On the other hand, most patients in the H5N1-positive group still showed rapid progress and deterioration of ARDS and died of respiratory failure, even with proper medical care followed by pathological investigation. Although aspartate aminotransferase and alanine aminotransferase levels were higher in the H5N1-positive but not the H5N1-negative group, the elevation of serum aminotransferase levels is a relatively common feature in H5N1 patients [6, 9, 25]. A

review of 2 groups of patients in large case studies has shown that elevated aminotransferase levels are not thought to be specific in H5N1 patients [26, 27]. These observations strongly suggest that H5N1-infected patients die because of rapidly progressive respiratory failure before revealing typical multiple organ failure status accompanied by failure of multiple organs such as liver, heart, and kidney.

Physiologically, we further analyzed data regarding the P/F ratio, which is a good parameter of oxygenation capacity for respiratory function. P/F ratios were <100 in both H5N1-positive and -negative patients, which means that the oxygenation capacity in both groups was severely damaged. Surprisingly, $PaCO_2$ levels revealed that ventilation capacity was normal in H5N1-positive patients but was severely damaged in H5N1-negative patients with ARDS; that is, H5N1-negative patients experienced more severe respiratory failure than did H5N1-positive patients on hospital admission. The log-rank test and the more severely conditioned Tarone-Ware test also showed a significant difference in survival probability between the H5N1-positive and H5N1-negative groups. H5N1-positive patients started with normal ventilation capacity on hospital admission, then rapidly proceeded to severe respiratory failure and death. Patients in the H5N1-positive group demonstrated a shorter duration until final outcome than patients in the H5N1-negative group; therefore, we designated these as fulminant ARDS patients. The initial check of blood gas levels may be an early diagnostic indicator of H5N1 infection. There may also be some mechanisms that influence cell activity during H5N1 infection and accelerate alveolar damage, resulting in death [28, 29]. Pathology and immunomodulator activity in H5N1 infection have been discussed elsewhere [30], but precise mechanisms have not been clarified yet [31].

Body temperature was significantly higher in H5N1-positive patients at the onset of disease, compared with H5N1-negative patients. This seasonal influenza-like symptom appears early in the course of the disease, with a body temperature >38°C in almost all infected patients [26]. Significant leukopenia and thrombocytopenia were observed in the H5N1-positive group ($P < .001$). Leukopenia and thrombocytopenia are observed in the majority of patients with H5N1 [26, 27]. There has been some discussion of the possibility that lymphopenia and increased levels of lactate dehydrogenase at presentation are associated with a poor prognosis [27]. Further investigation into lymphopenia and liver function in H5N1 patients is necessary for clarification.

We have demonstrated here that H5N1 infection with ARDS starts with high fever but relatively mild respiratory symptoms, then proceeds to serious respiratory failure with lower survival probability and shorter periods of illness (fulminant ARDS), compared with ARDS without H5N1 infection. Leukopenia, thrombocytopenia, and liver function on hospital admission might be risk parameters and early indicators of patients with H5N1 influenza virus infection.

Acknowledgments

We thank a coordinator, Ms. Yen, and all members of the NHP and the Ministry of Health in Vietnam for their cooperation.

References

1. Shortridge KF, Zhou NN, Guan Y, et al. Characterization of avian H5N1 influenza viruses from poultry in Hong Kong. Virology **1998**; 252:331–42.
2. Bridges CB, Katz JM, Seto WH, et al. Risk of influenza A (H5N1) infection among health care workers exposed to patients with influenza A (H5N1), Hong Kong. J Infect Dis **2000**; 181:344–8.
3. Peiris JSM, Yu WC, Leung CW, et al. Re-emergence of fatal human influenza A subtype H5N1 disease. Lancet **2004**; 363:617–9.
4. WHO guidelines for the global surveillance of severe acute respiratory syndrome (SARS). Updated recommendations, October **2004**.
5. Peiris JS, Lai ST, Poon LL, et al; SARS study group. Coronavirus as a possible cause of severe acute respiratory syndrome. Lancet **2003**; 361: 1319–25.
6. Hien TT, Liem NT, Dung NT, et al; for the World Health Organization International Avian Influenza Investigative Team, Farraret J. Avian influenza A (H5N1) in 10 patients in Vietnam. N Engl J Med **2004**; 350: 1179–88.
7. Ungchusak K, Auewarakul P, Dowell SF, et al. Probable person-to-person transmission of avian influenza A (H5N1). N Engl J Med **2005**; 352: 333–40.
8. Apisarnthanarak A, Kitphati R, Thongphubeth K, et al. Atypical avian influenza (H5N1). Emerg Infect Dis **2004**; 10:1321–4.
9. Chotpitayasunondh T, Ungchusak K, Hanshaoworakul W, et al. Human disease from influeanza A (H5N1), Thailand, 2004. Emerg Infect Dis **2005**; 11:201–9.
10. Uiprasertkul M, Puthavathana P, Sangsiriwut K, et al. Influenza H5N1 replication sites in humans. Emerg Infect Dis **2005**; 11:1036–41.
11. Oner AF, Bay A, Arslan S, et al. Avian influenza A (H5N1) infection in eastern Turkey in 2006. N Engl J Med **2006**; 355:2179–85.
12. Kandun N, Wibisono H, Sedyaningsih ER, et al. N Engl J Med **2006**;355: 2186–94.
13. Sedyaningsih ER, Isfandari S, Setiawaty V, et al. Epidemiology of cases of H5N1 virus infection in Indonesia, July 2005-June 2006. J Infect Dis **2007**; 196:522–7.
14. Kandun N, Tresnaningsih E, Purba WH, et al. Factors associated with case fatality of human H5N1 virus infections in Indonesia: a case series. Lancet **2008**; 372:744–9.
15. Anderson MR. Update on pediatric acute respiratory distress syndrome. Respir Care **2003**; 48:261–78.
16. The Writing Committee of the World Health Organization Consultation (WHO) on Human Influenza A/H5. Avian influenza A (H5N1) infection in humans. N Engl J Med **2005**; 353:1374–85.
17. Liem NT, Nakajima N, Phat lP, et al. H5N1-Infected cells in lung with diffuse alveolar damage in exudative phase from a fatal case in Vietnam. Jpn J Infect Dis **2008**; 61:157–60.
18. Korteweg C, Gu J. Pathology, molecular biology, and pathogenesis of avian influenza A (H5N1) infection in humans. Am J Pathol **2008**; 172:1155–70.
19. Marmel LA. Pandemic avian influenza. Lancet Infect Dis **2005**; 5:666–7.
20. McFee, RB. Avian influenza: the next pandemic? Dis Mon **2007**; 53: 348–7.
21. Bernard GR, Artigas A, Brigham KL, et al. The American-European

consensus conference on ARDS: definitions, mechanisms, relevant outcomes, and clinical trial coordination. Am J Respir Crit Care Med **1994**; 149:818–24.
22. Flori HR, Glidden DV, Rutherford GW, Matthay MA. Pediatric acute lung injury: prospective evaluation of risk factors associated with mortality. Am J Respir Crit Care Med **2005**; 171:995–1001.
23. Ware LB, Matthay MA. The acute respiratory distress syndrome. N Engl J Med **2000**; 342:1334–49.
24. Bernard G. Acute respiratory distress syndrome: a historical perspective. Am J Respir Crit Care Med **2005**; 172:798–806.
25. Yu H, Shu Y, Hu S, et al. The first confirmed human case of avian influenza A (H5N1) in mainland China. Lancet **2006**; 367:84.
26. Arabi Y, Gomersall CD, Ahmed QA, Boynton BR, Memish ZA. The critically ill avian influenza A (H5N1) patient. Crit Care Med **2007**; 35:1397–403.
27. Writing Committee of the Second World Health Organization Consultation on Clinical Aspects of Human Infection with Avian Influenza A (H5N1) Virus. Update on avian influenza A (H5N1) virus infection in humans. N Engl J Med **2008**; 358:261–73.
28. Daidoji T, Koma T, Du A, et al. H5N1 avian influenza virus induces apoptotic cell death in mammalian airway epithelial cells. J Virol **2008**; 82:11294–307.
29. Imai Y, Kuba K, Neely GG, et al. Identification of oxidative stress and toll-like receptor 4 signaling as a key pathway of acute lung injury. Cell **2008**; 133:235–49.
30. Gu J, Xie Z, Gao Z, et al. H5N1 infection of the respiratory tract and beyond: a molecular pathology study. Lancet **2007**; 370:1137–45.
31. Korteweg C, Gu J. Pathology, molecular biology, and pathogenesis of avian influenza A (H5N1) infection in humans. Am J Pathol **2008**; 172:1155–70.

Cytoprotective Function of Heme Oxygenase 1 Induced by a Nitrated Cyclic Nucleotide Formed during Murine Salmonellosis[1]

Mohammad Hasan Zaki, Shigemoto Fujii, Tatsuya Okamoto, Sabrina Islam, Shahzada Khan, Khandaker Ahtesham Ahmed, Tomohiro Sawa, and Takaaki Akaike[2]

Signaling mechanisms of NO-mediated host defense are yet to be elucidated. In this study, we report a unique signal pathway for cytoprotection during *Salmonella* infection that involves heme oxygenase 1 (HO-1) induced by a nitrated cyclic nucleotide, 8-nitroguanosine 3′,5′-cyclic monophosphate (8-nitro-cGMP). Wild-type C57BL/6 mice and C57BL/6 mice lacking inducible NO synthase (iNOS) were infected with *Salmonella enterica* serovar Typhimurium LT2. HO-1 was markedly up-regulated during the infection, the level being significantly higher in wild-type mice than in iNOS-deficient mice. HO-1 up-regulation was associated with 8-nitro-cGMP formation detected immunohistochemically in *Salmonella*-infected mouse liver and peritoneal macrophages. 8-Nitro-cGMP either exogenously added or formed endogenously induced HO-1 in cultured macrophages infected with *Salmonella*. HO-1 inhibition by polyethylene glycol-conjugated zinc-protoporphyrin IX impaired intracellular killing of bacteria in mouse liver and in both RAW 264 cells and peritoneal macrophages. Infection-associated apoptosis was also markedly increased in polyethylene glycol-conjugated zinc-protoporphyrin IX-treated mouse liver cells and cultured macrophages. This effect of HO-1 inhibition was further confirmed by using HO-1 short interfering RNA in peritoneal macrophages. Our results suggest that HO-1 induced by NO-mediated 8-nitro-cGMP formation contributes, via its potent cytoprotective function, to host defense during murine salmonellosis. *The Journal of Immunology,* 2009, 182: 3746–3756.

Nitric oxide produced by inducible NO synthase (iNOS)[3] during infection and inflammation plays a crucial role in host defense mechanisms via its antimicrobial (1, 2), cytoprotective (3, 4), and immunoregulatory (5) activities. NO-mediated host defense is imparted mainly by reactive nitrogen oxide species (RNS) such as nitrogen dioxide (NO_2) and peroxynitrite ($ONOO^-$), which are produced by means of reaction with reactive oxygen species (ROS), especially superoxide (O_2^-) and hydrogen peroxide (H_2O_2), in phagocytic systems such as macrophages and polymorphonuclear leukocytes (6). RNS thus formed can modify both microbial and host proteins, lipids, and nucleic acids, thereby generating nitrative stress during infection and inflammation (7–10). Formation of 3-nitrotyrosine is one of the most commonly identified biomarkers for RNS generation that has been observed in a number of diseases and experimental conditions (11–13). RNS-induced nitration is known to occur not only with amino acids and proteins but also with nucleic acids. For example, formation of 8-nitroguanine or 8-nitroguanosine and their derivatives has been observed both in vitro and in vivo (13–17). 8-Nitroguanosine has a redox active property (18, 19), which suggests that nucleotide nitration may have a biological function rather than simply being a biological marker. In this context, we recently discovered a nitrated cyclic nucleotide, 8-nitroguanosine 3′,5′-cyclic monophosphate (8-nitro-cGMP), which is formed in physiological systems and may be involved in redox activity and signal transduction (20). The signaling function of 8-nitro-cGMP appears to be mediated by its unique reaction with the sulfhydryl group of cysteines, thus forming a protein *S*-cGMP adduct, which is an important mechanism of posttranslational modification of proteins that we have named protein *S*-guanylation (20).

NO has critical functions for cellular signaling mechanisms. An important signal induced by NO is heme oxygenase 1 (HO-1), a rate-limiting enzyme and a significant cytoprotective molecule produced under physiological conditions and by different stresses, including oxidative stress (21–27), endotoxemia (28), UV irradiation (29), heavy metals (30), heat shock (31), and NO (22–27). The main function of HO-1 is to degrade heme to form Fe(II), biliverdin, and carbon monoxide (CO) (21). Biliverdin is subsequently converted to bilirubin by biliverdin reductase (32). These catalytic products of HO-1 seem to have various physiological roles. For example, bilirubin (converted from biliverdin) acts as a potent antioxidant because of free radical scavenging properties (32, 33); the other product (CO) is thought to contribute to vasoregulation (34, 35), cytoprotection (36, 37), anti-inflammatory

Department of Microbiology, Graduate School of Medical Sciences, Kumamoto University, Kumamoto, Japan

Received for publication October 7, 2008. Accepted for publication January 8, 2009.

The costs of publication of this article were defrayed in part by the payment of page charges. This article must therefore be hereby marked *advertisement* in accordance with 18 U.S.C. Section 1734 solely to indicate this fact.

[1] This work was supported in part by Grants-in-Aid for scientific research from the Ministry of Education, Culture, Sports, Science and Technology and the Ministry of Health, Labor and Welfare of Japan.

[2] Address correspondence and reprint requests to Prof. Takaaki Akaike, Department of Microbiology, Graduate School of Medical Sciences, Kumamoto University, 860-8556 Kumamoto, Japan. E-mail address: takakaik@gpo.kumamoto-u.ac.jp

[3] Abbreviations used in this paper: iNOS, inducible NO synthase; 8-bromo-cGMP, 8-bromoguanosine 3′,5′-cyclic monophosphate; GSNO, *S*-nitrosoglutathione; HO-1, heme oxygenase 1; H_2-DCFDA, 2′,7′-dichlorodihydrofluorescein diacetate, diacetoxymethylester; Keap1, Kelch-like ECH-associated protein 1; L-NIL, N^6-(1-iminoethyl)-L-lysine; L-NMMA, N^ω-monomethyl-L-arginine; MOI, multiplicity of infection; 8-nitro-cGMP, 8-nitroguanosine 3′,5′-cyclic monophosphate; NOC7, 3-(2-hydroxy-1-methyl-2-nitrosohydrazino)-*N*-methyl-1-propanamine; Nrf2, NF-E2-related factor 2; PEG-ZnPP, polyethylene glycol-conjugated zinc protoporphyrin IX; RNS, reactive nitrogen oxide species; ROS, reactive oxygen species; siRNA, short interfering RNA; SNAP, *S*-nitroso-*N*-acetyl-D,L-penicillamine; 15d-PGJ_2, 15-deoxy-$\Delta^{12,14}$-PGJ_2; 8-bromo-cGMP, 8-bromoguanosine 3′5′-cyclic monophosphate.

www.jimmunol.org/cgi/doi/10.4049/jimmunol.0803363

effects (38, 39), and inhibition of T cell proliferation (40). In fact, HO-1 protects against cell and tissue damage induced by LPS both in vitro and in vivo (24, 28). We have also demonstrated that, in several solid tumor models, expression of HO-1 in tumor cells that was up-regulated by NO could contribute to tumor growth, possibly because of potent cytoprotective activity (26, 27, 41, 42). Although host cell apoptosis induced by various pathogens and microbial toxins is critical in the pathogenesis of many infectious diseases, no study has yet confirmed the antiapoptotic and host defense roles of HO-1 during bacterial infections in vivo.

The host defense effects of NO have been reported for many microbiological infections including leishmaniasis (5), tuberculosis (43, 44), salmonellosis (2, 44–49), and listeriosis (50). Murine salmonellosis has been studied extensively so as to investigate host defense mechanisms and immune responses occurring during typhoid fever: the infection induces excessive production of NO as a host defense response (2, 44–49). In earlier studies, we found much greater bacterial growth and apoptotic changes in iNOS-deficient ($iNOS^{-/-}$) mice than in wild-type mice ($iNOS^{+/+}$) during *Salmonella* infection (2, 45, 46, 49). However, the mechanism of NO-mediated cytoprotection that occurred during *Salmonella* infection remained unclear.

In the present experiments, we sought to clarify NO-dependent cytoprotective and antimicrobial host defense, with a particular focus on the signaling mechanism of HO-1 induction as a cytoprotective response for *Salmonella enterica* serovar Typhimurium (*S. typhimurium*) infection in vivo and in vitro. We also investigated formation of 8-nitro-cGMP in *Salmonella*-infected mouse liver cells and macrophages in culture and its possible signaling role in the cytoprotective host defense mediated by HO-1 induction.

Materials and Methods

Animals

Littermates of wild-type C57BL/6 mice and C57BL/6-NOS2$^{-/-}$ ($iNOS^{-/-}$) mice were used throughout the study, conducted according to the guidelines in the Laboratory Protocol of Animal Handling, Kumamoto University Graduate School of Medical Sciences.

Bacterial infection in mice

The bacteria S. *typhimurium* LT2 were used throughout the study. Bacteria were grown in still culture of brain-heart infusion broth (Difco Laboratories). The bacterial suspension was prepared in 10 mM PBS (pH 7.4) and inoculum doses were adjusted by measuring the OD of the bacterial suspension at 620 nm. Mice were infected by i.p. injection of 0.1 ml of the bacteria-PBS suspension containing 1×10^4, or 2×10^4, or 4×10^4 CFU.

Treatment of Salmonella*-infected mice with HO-1 inhibitor*

To inhibit HO-1 activity, mice were treated with polyethylene glycol-conjugated zinc-protoporphyrin (PEG-ZnPP) diluted in physiological saline. PEG-ZnPP, a water-soluble derivative of HO-1 inhibitor ZnPP IX, was synthesized according to our method reported previously (51). Mice were given 0.1 ml of 1 mM PEG-ZnPP (equivalent to 2.5 mg of ZnPP IX/kg of body weight) once daily via tail vein at days 0, 1, 2, and 3 after bacterial infection. Mice treated in the same manner but with only the vehicle (PBS) served as controls.

Measurement of bacterial growth in liver

Livers were collected at scheduled intervals, and liver homogenate samples were prepared as described elsewhere (45) and subjected to the colony formation assay according to the standard method (45).

Cell culture

The murine macrophage-like cell line RAW 264 and peritoneal macrophages were cultured in DMEM containing 10% heat-inactivated FCS (Sigma-Aldrich) at 37°C under 5% CO_2. Peritoneal macrophages were harvested via peritoneal lavage of thioglycolate-elicited peritoneal exudate from wild-type and $iNOS^{-/-}$ mice, and macrophages were isolated by removing nonadherent cells in culture, as reported recently (46). For the study of HO-1 induction by NO, either *S*-nitroso-*N*-acetyl-D,L-penicillamine (SNAP) or other NO donors were added to cell cultures at desired concentrations. For inhibition of iNOS, cells were treated with either N^{ω}-monomethyl-L-arginine (L-NMMA) or N^6-(1-iminoethyl)-L-lysine (L-NIL) for 12 h before infection and 1 h after gentamicin treatment.

Transfection of short interfering RNA (siRNA)

A 25-nt HO-1 siRNA (sense, UUACAUGGCAUAAAUUCCCACUGCC; antisense, GGCAGUGGGAAUUUAUGCCAUGUAA), manufactured by Invitrogen, was used for transfection with Lipofectamine 2000 transfection reagent (Invitrogen). Cultured peritoneal macrophages were transfected with siRNA at a final concentration of 100 nM for 48 h. Stealth RNAi Negative Control (low GC; Invitrogen) was used as control siRNA.

Infection of macrophages

RAW 264 cells and mouse peritoneal macrophages were infected as described earlier (46). Briefly, bacteria grown in brain-heart infusion broth overnight were washed and opsonized with 10% normal mouse serum for 30 min at 37°C. Bacterial suspension was added to 24-well plate at a multiplicity of infection (MOI) of 10 and centrifuged at $130 \times g$ for 5 min to synchronize the infection, followed by incubation at 37°C for 30 min.

Macrophage bactericidal assay

Intracellular *Salmonella* killing was examined with RAW 264 cells and peritoneal macrophages as described earlier (46). After infection, cells were washed with prewarmed PBS and incubated for 1 h at 37°C with DMEM containing 100 μg/ml gentamicin, followed by incubation with DMEM containing 10 μg/ml gentamicin. To investigate the effect of HO-1 inhibition on bacterial growth, 20 μM PEG-ZnPP was added to the cultures at 12 h before infection and 1 h after gentamicin treatment. At 6, 12, and 24 h after infection, cells were washed twice with PBS and lysed with 0.1% Triton X-100. Serially diluted cell lysates were subjected to the colony formation assay for quantification of intracellular bacteria. To obtain bacterial count in siRNA-transfected cells, cells were collected in DMEM after washing twice with PBS and counted the number of cells followed by centrifugation and lysis with 0.1% Triton X-100 for colony assay. Bacterial count was adjusted with the number of cells because HO-1 siRNA-transfected cells tended to washout from the plate compared with control siRNA.

Immunohistochemistry and immunocytochemistry

Liver tissues and cultured cells were fixed and cryostat tissue sections were prepared as described earlier (20, 45). Immunostaining was achieved by using biotin-conjugated monoclonal mouse Abs for 8-nitro-cGMP (clones 1G6 and 1H7) and by using rabbit polyclonal anti-HO-1 IgG (Stressgen Biotechnologies), as reported in a recent publication (17, 20). For immunofluorescence staining for 8-nitro-cGMP, Abs were labeled with Alexa Fluor 555 (Molecular Probes-Invitrogen). Images were obtained by means of an Olympus DP70 digital camera and software.

Apoptosis assay

Apoptosis in mouse liver tissues infected with *S. typhimurium* was analyzed by use of the TUNEL assay with an in situ apoptosis detection kit (TACS; Trevigen), as described previously (45, 46). For in vitro TUNEL analysis, RAW 264 cells and peritoneal macrophages were cultured at densities of 2×10^5 and 5×10^5 cells/well of 4-well chamber slides, respectively. At 12 h after infection, cells were washed twice with PBS and fixed with 3.7% buffered formaldehyde for 15 min at room temperature.

Western blot analysis

Western blotting was performed according to our standard procedure (20), unless otherwise specified. The tissue homogenate and cell lysate protein samples were separated via SDS-PAGE (12%), followed by electroblotting to polyvinylidene fluoride membranes. Membranes were subjected to immunoblotting with rabbit polyclonal anti-HO-1 Ab (Stressgen Biotechnologies). Caspase 3 and cytochrome *c* were detected by means of rabbit polyclonal anti-cleaved caspase 3 (ASP175; Cell Signaling Technology) and rabbit polyclonal anti-cytochrome *c* (H-104; Santa Cruz Biotechnology), respectively.

Measurement of CO in blood

We estimated CO production of RBC by measuring hemoglobin-associated CO in blood from *Salmonella*-infected mice. Specifically, 350 μl of freshly collected mouse blood was diluted with 3.65 ml of PBS in a 10-ml test tube

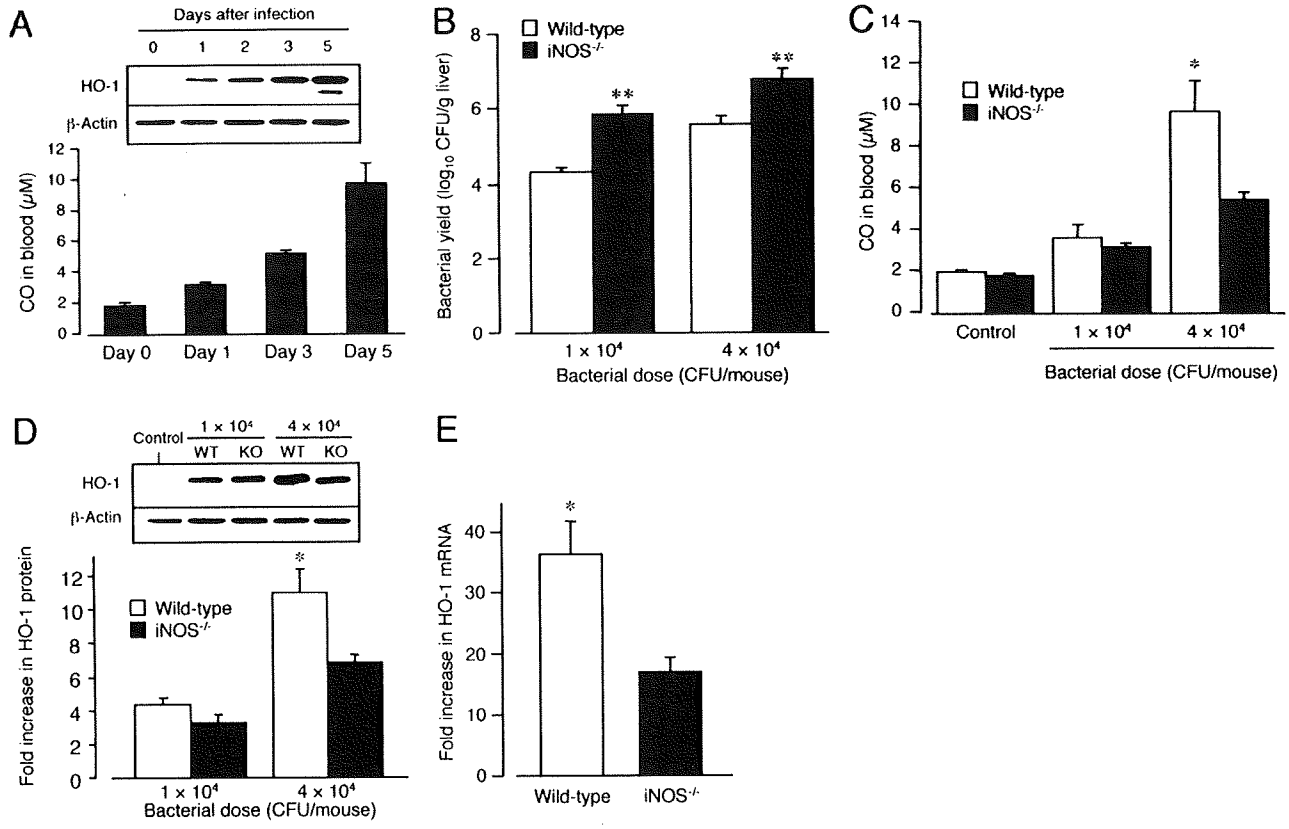

FIGURE 1. Induction of HO-1 during murine salmonellosis. *A*, Wild-type (WT) mice were infected with *S. typhimurium* at a dose of 4×10^4 CFU/mouse, after which the blood CO level was determined. The blood CO level was also determined for uninfected wild-type mice (control). Data are means ± SEM (n = 3–5). *Inset* shows Western blot analysis of HO-1 in livers. *B*, Wild-type and iNOS$^{-/-}$ mice were infected with *S. typhimurium* at a dose of 1×10^4 or 4×10^4 CFU/mouse, and bacterial yield in livers at day 5 after infection was measured as stated above. Data are means ± SEM (n = 5 or 6 of at least two independent experiments). **, $p < 0.01$ vs wild-type mice (unpaired Student's t test). *C*, CO in blood from wild-type and iNOS$^{-/-}$ mice at day 5 after *S. typhimurium* infection. Data are means ± SEM (n = 3–5). *D*, Increase in HO-1 protein expression in livers from wild-type and iNOS$^{-/-}$ mice 5 days after infection with different bacterial doses. *Inset* shows Western blotting results. Relative band intensity of HO-1 protein was normalized to that of β-actin. Data are means ± SEM (n = 5 or 6). *E*, Increase in HO-1 mRNA expression in livers from wild-type and iNOS$^{-/-}$ mice quantified via real-time RT-PCR 5 days after infection (4×10^4 CFU). Data are means ± SEM (n = 6). *C–E*: *, $p < 0.05$ vs iNOS$^{-/-}$ (unpaired Student's t test). KO, Knockout.

sealed with an airtight rubber cap. To remove residual oxygen gas from the solution in the tube, nitrogen gas was forced into the solution for 2 min via a needle inserted through the rubber cap. As the source of NO, 40 μl of 0.1 M 3-(2-hydroxy-1-methyl-2-nitrosohydrazino)-*N*-methyl-1-propanamine (NOC7; Dojindo Laboratories) was added to the solution, and the sample was incubated for 2 h at room temperature under anaerobic conditions. Because NO has greater affinity for heme iron than does CO, exogenously added NO effectively replaces hemoglobin-bound CO, and CO purged from heme accumulates in the gaseous phase in the tube. After NO treatment, each aliquot in the tube was injected into a gas chromatography-based biogas analyzer (Taiyo Instruments) to measure the CO content. In fact, using CO-saturated hemoglobin, we confirmed that almost 100% of CO bound with hemoglobin was recovered in the gaseous phase.

Quantification of HO-1 mRNA expression

Expression of HO-1 mRNA was quantified by real-time RT-PCR analysis. Total RNA was isolated by use of TRIzol reagent (Invitrogen). cDNA was synthesized using 2.5 μg of RNA in a reaction mixture of 20 μl containing 1.0 μl of 10 U/μl RNase inhibitor, 1.0 μl of 3 μg/μl random primer, and 1.0 μl of 200 U/μl Moloney murine leukemia virus reverse transcriptase. Real-time RT-PCR was performed by using an Applied Biosystems Prism 7700 Real-Time PCR System with TaqMan Universal PCR master mix and Assays-on-Demand gene expression probes (Applied Biosystems). The amount of mRNA was quantified by means of the standard curve method. A standard sample was serially diluted and used for constructing this standard curve. Simultaneous quantification of 18S rRNA, with TaqMan Rodent 18S rRNA Control Reagents VIC (Applied Biosystems) was used as an endogenous control to normalize the differences in reverse transcription efficiencies and amount of template in the reaction mixture.

Measurement of ROS

The intracellular ROS level was assessed with 2′,7′-dichlorodihydrofluorescein diacetate, diacetoxymethylester (H_2-DCFDA; Molecular Probes) as described earlier (42). After macrophages were incubated with H_2-DCFDA, 2′,7′-dichlorofluorescein fluorescence intensity was measured via a flow cytometer (BD Biosciences).

Statistical analysis

All data are presented as means ± SEM or SD. Statistical significance between two groups was determined by means of a two-tailed unpaired Student's t test. A value of $p < 0.05$ was considered statistically significant.

Results

HO-1 expression induced by NO during Salmonella *infection in vivo*

We first examined whether HO-1 is up-regulated in murine salmonellosis by infecting wild-type mice with *S. typhimurium* LT2. At days 1–5 after infection, mouse livers were collected for analysis of HO-1 expression. In vivo HO-1 activity, as evidenced by CO produced in the blood, increased in a time-dependent fashion (Fig. 1*A*), in parallel with growth of *Salmonella* organisms in the liver (bacterial yield ($\log_{10}$ CFU/g liver); 4.1 ± 0.2 (day 1), 5.1 ± 0.3 (day 3), 6.1 ± 0.2 (day 5)). HO-1 expression in mouse liver induced by *S. typhimurium* infection was further confirmed via

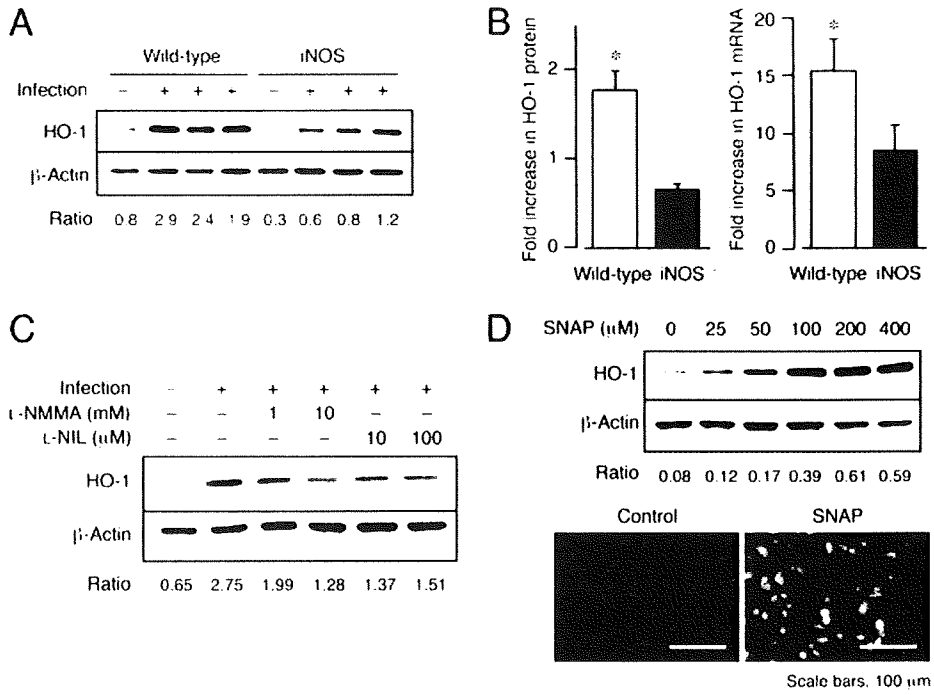

FIGURE 2. NO-dependent HO-1 induction in *S. typhimurium*-infected macrophages from wild-type and iNOS$^{-/-}$ mice. *A*, Cultured macrophages were infected with *S. typhimurium* at 10 MOI. Western blotting detected HO-1 expression at 24 h after infection. Data from three cultures are shown. *B*, HO-1 protein and mRNA expression in macrophages. Data are means ± SD ($n = 3$). *, $p < 0.05$ vs iNOS$^{-/-}$ (unpaired Student's t test). *C*, Wild-type macrophages were infected with *S. typhimurium* at 10 MOI. Cells were treated with either L-NMMA or L-NIL at 12 h before infection, and HO-1 expression at 24 h after infection was measured by Western blotting. *D*, Macrophages from iNOS$^{-/-}$ mice were treated with SNAP for 12 h. Western blotting and immunocytochemistry show HO-1 expression. The relative intensity of HO-1 vs β-actin is shown at the bottom (*C* and *D*).

Western blot analysis for HO-1 (Fig. 1*A*, *inset*) and immunostaining for HO-1 protein (data not shown). Induction of HO-1 activity in the liver was also confirmed by measuring the production of biliverdin spectrophotometrically as reported earlier (27) (data not shown).

We then investigated the effect of NO on HO-1 induction in livers of infected mice. Both wild-type and iNOS$^{-/-}$ mice were injected with *S. typhimurium* LT2 at a dose of either 1×10^4 CFU/mouse (low dose) or 4×10^4 CFU/mouse (high dose). On day 5 after infection, the livers from iNOS$^{-/-}$ mice had significantly higher bacterial growth than did livers from wild-type mice, regardless of the *S. typhimurium* dose (Fig. 1*B*). In contrast, HO-1 activity, as evidenced by CO production (Fig. 1*C*), HO-1 protein (Fig. 1*D*), and HO-1 mRNA (Fig. 1*E*) were higher in wild-type mice than in iNOS$^{-/-}$ mice. Even under the conditions where similar bacterial yields were detected (wild-type mice at high dose vs iNOS$^{-/-}$ mice at low dose in Fig. 1*B*), a significantly higher HO-1 activity (Fig. 1*C*) and expression (Fig. 1, *D* and *E*) were determined for wild-type mice than for iNOS$^{-/-}$ mice. These findings suggest that NO derived from iNOS plays an important role in HO-1 induction during *Salmonella* infection.

Cells expressing HO-1 were identified by double immunostaining with Abs for HO-1 and macrophages or neutrophils. Most macrophages were positive for HO-1, whereas some but not all neutrophils were HO-1 positive (data not shown). Microscopic observation revealed that hepatocytes did not have strong staining for HO-1, although a weak immunoreaction was observed in *Salmonella*-infected liver compared with control liver.

HO-1 expression induced by NO in Salmonella*-infected macrophages in culture*

NO-dependent HO-1 induction in macrophages was investigated in more detail by means of an in vitro study using peritoneal macrophages from both wild-type and iNOS$^{-/-}$ mice. These peritoneal macrophages were infected with *S. typhimurium* at a MOI of 10, and 24 h after infection HO-1 expression was determined by Western blotting and real-time RT-PCR. Consistent with in vivo results, macrophages from wild-type mice had significantly higher HO-1 protein and mRNA levels than macrophages from iNOS$^{-/-}$ mice during *Salmonella* infection (Fig. 2, *A* and *B*). Treatment of *S. typhimurium*-infected wild-type macrophages with a NOS inhibitor, L-NMMA or L-NIL, resulted in a significant reduction in HO-1 expression (Fig. 2*C*).

NO-mediated induction of HO-1 in *Salmonella*-infected macrophages was also examined by using exogenous NO donors. Uninfected iNOS$^{-/-}$ peritoneal macrophages were incubated with different concentrations of the NO donors SNAP, *S*-nitrosoglutathione (GSNO), and NOC7. HO-1 induction was assessed via Western blot and immunocytochemistry at 12 h after treatment with these NO donors. HO-1 was markedly induced by SNAP (Fig. 2*D*) and by other NO donors such as GSNO and NOC7 (data not shown) in a dose-dependent manner. Similarly, when iNOS$^{-/-}$ peritoneal macrophages infected with *Salmonella* were treated with 200 μM NOC7, GSNO, or SNAP, the HO-1 level was higher in cells treated with the NO donors than in untreated cells (data not shown).

Upon bacterial infection, it is known that phagocytic oxidase (Phox; NADPH oxidase, Nox) is activated to generate ROS (47, 48, 52, 53). We measured ROS generation during *Salmonella* infection by using oxidant-sensitive probe (H_2-DCFDA). This analysis showed that similar levels of ROS were generated in wild-type and iNOS$^{-/-}$ macrophages early in the infection (i.e., at 6 h; data not shown), although the amount of ROS tended to be higher in iNOS$^{-/-}$ macrophages than in wild-type macrophages at a later time (at 24 h; data not shown). In addition, similar to the in vivo results (Fig. 1*B*), the number of bacteria grown intracellularly was significantly higher for iNOS$^{-/-}$ macrophages than for wild-type cells (data not shown).

These results strongly support the interpretation mentioned earlier of NO-dependent HO-1 induction during *Salmonella* infection.

Formation of 8-nitro-cGMP and its signaling functions during murine salmonellosis

We recently reported formation of 8-nitro-cGMP in immunostimulated mouse macrophages in culture (20). We also determined that

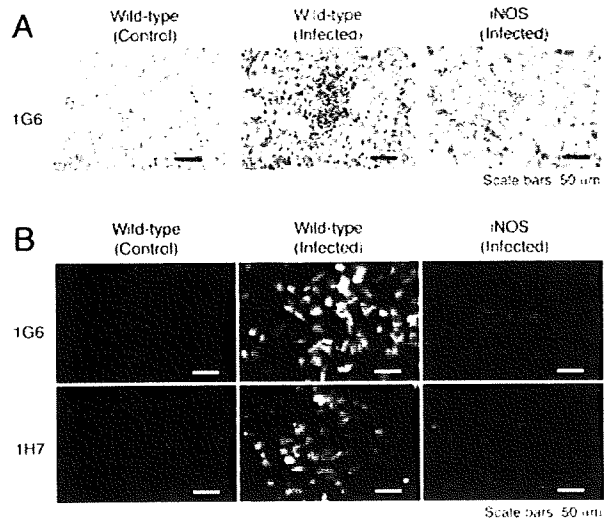

FIGURE 3. HO-1 induction and formation of 8-nitro-cGMP in *S. typhimurium*-infected mouse liver and peritoneal macrophages. *A*, Wild-type and iNOS$^{-/-}$ mice were infected with *S. typhimurium* at a dose of 4×10^4 CFU/mouse. Liver sections from uninfected wild-type mice (control; day 0) and *Salmonella*-infected wild-type and iNOS$^{-/-}$ mice at day 5 were fixed and processed for immunostaining with 1G6 Ab. *B*, Peritoneal macrophages from wild-type and iNOS$^{-/-}$ mice were seeded at a density of 5×10^5 cells/well in 4-well chamber slides and were infected with *S. typhimurium* at 10 MOI. At 24 h after infection, cells were fixed and stained with either 1G6 or 1H7 Ab. Uninfected macrophages from wild-type mice served as control.

8-nitro-cGMP reacts with the sulfhydryl group of proteins and forms protein-cysteine-cGMP adducts by a process that we called *S*-guanylation (20). *S*-Guanylation of proteins by 8-nitro-cGMP is a new concept in cell biology and may have a significant role in unique posttranslational modification of proteins. More important, in this earlier work we reported that transcription of phase 2 antioxidant enzymes including HO-1 involved 8-nitro-cGMP-dependent *S*-guanylation of Kelch-like ECH-associated protein 1 (Keap1), a cysteine-rich redox-sensitive regulatory protein involved in sequestration of transcription factor NF-E2-related factor 2 (Nrf2).

To study mechanisms how NO can mediate HO-1 expression during *Salmonella* infection, we focused on 8-nitro-cGMP formation. For immunochemical detection of 8-nitro-cGMP, we produced two different clones of mAbs, 1G6 and 1H7. Clone 1G6 detected 8-nitro-cGMP and 8-nitroguanosine, whereas 1H7 was specific for 8-nitro-cGMP. Wild-type and iNOS$^{-/-}$ mice infected with *S. typhimurium* at a dose of 4×10^4 were used for these studies at day 5 after infection. We observed strong immunoreactivity for 1G6 Ab in *Salmonella*-infected wild-type mouse liver but not in uninfected wild-type mouse liver (control; day 0) and infected iNOS$^{-/-}$ mouse liver (Fig. 3*A*). We found similar results in an in vitro study with peritoneal macrophages from wild-type and iNOS$^{-/-}$ mice: strong immunostaining for both 1G6 and 1H7 in infected wild-type macrophages but almost no immunostaining in uninfected wild-type and infected iNOS$^{-/-}$ macrophages (Fig. 3*B*).

We also investigated, via immunocytochemical methods, the possible association of 8-nitro-cGMP formation with induction of HO-1 during *S. typhimurium* infection in peritoneal macrophages from wild-type mice. Double immunofluorescence staining for 8-nitro-cGMP and HO-1 at 24 h after infection revealed HO-1 expression in almost the same location as that for 8-nitro-cGMP (data not shown).

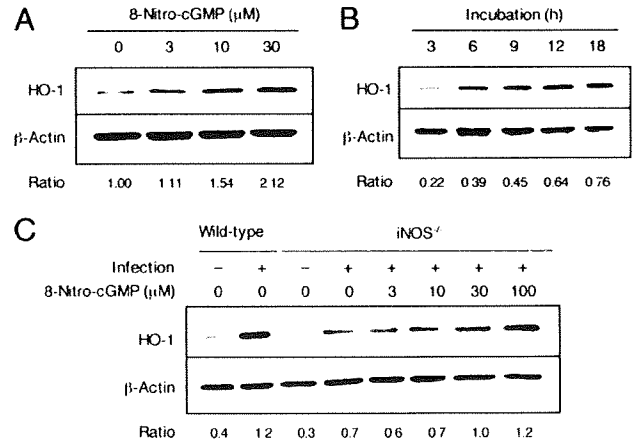

FIGURE 4. Induction of HO-1 by 8-nitro-cGMP. *A*, 8-Nitro-cGMP at various concentrations was added to peritoneal macrophages from iNOS$^{-/-}$ mice and, 12 h after treatment, HO-1 expression was measured by means of Western blotting. *B*, After 30 μM 8-nitro-cGMP was added to peritoneal macrophages from iNOS$^{-/-}$ mice, HO-1 expression was measured via Western blotting. *C*, Peritoneal macrophages from wild-type and iNOS$^{-/-}$ mice were infected with *S. typhimurium* at 10 MOI. Six hours after infection, 8-nitro-cGMP at different concentrations was added to the infected iNOS$^{-/-}$ macrophages. At 24 h after infection, HO-1 expression was measured by using Western blotting. Each blot represents at least three independent experiments. The relative intensity of HO-1 vs β-actin is shown at the bottom.

8-Nitro-cGMP as a second messenger in NO-mediated HO-1 induction

We then investigated the possible signaling function of 8-nitro-cGMP in HO-1 induction during *Salmonella* infection. The HO-1 induction potential of 8-nitro-cGMP was examined by adding chemically synthesized 8-nitro-cGMP to uninfected iNOS$^{-/-}$ macrophage cultures. Marked, dose-dependent induction of HO-1 was seen in iNOS$^{-/-}$ macrophages and was highest between 12 and 18 h (Fig. 4, *A* and *B*). We then treated *Salmonella*-infected iNOS$^{-/-}$ macrophages with 8-nitro-cGMP and measured HO-1 induction at 24 h after infection via Western blot analysis. Fig. 4*C* shows that *Salmonella*-infected iNOS$^{-/-}$ macrophages had reduced expression of HO-1 compared with that of wild-type-infected macrophages, but the decreased HO-1 expression was almost restored by 30–100 μM 8-nitro-cGMP treatment. This observation clearly demonstrated that 8-nitro-cGMP, which forms in wild-type macrophages during *Salmonella* infection, has a signaling function as a second messenger of NO in HO-1 induction.

Impaired host defense against Salmonella *caused by HO-1 antidotes*

To address whether HO-1 induced by NO possesses host defense functions during *S. typhimurium* infection, we tested the effect of HO-1 inhibition on bacterial growth in wild-type mice by treating infected mice with PEG-ZnPP at a dose that was equivalent to 2.5 mg of ZnPP IX/kg of body weight. We used three bacterial doses (1×10^4, 2×10^4, and 4×10^4 CFU/mouse). PEG-ZnPP treatment started after infection of bacteria and continued until day 3 after infection. At day 5 after infection, we determined blood CO levels (Fig. 5*A*) and the number of bacteria in liver samples (Fig. 5*B*). PEG-ZnPP treatment effectively inhibited HO-1 activity, as evidenced by reduced CO levels for PEG-ZnPP-treated groups compared with controls, at all three bacterial doses (Fig. 5*A*), the difference being significant ($p < 0.05$) for the two higher bacterial